Chemical Geology 351 (2013) 115–133

Contents lists available at SciVerse ScienceDirect

Chemical Geology

journal homepage: www.elsevier.com/locate/chemgeo

Serpentinization and carbon sequestration: A study of two ancient peridotite-hosted hydrothermal systems

Esther M. Schwarzenbach [a,*,1], Gretchen L. Früh-Green [a], Stefano M. Bernasconi [b], Jeffrey C. Alt [c], Alessio Plas [a]

[a] Institute of Geochemistry and Petrology, ETH Zurich, CH-8092 Zurich, Switzerland
[b] Geological Institute, ETH Zurich, CH-8092 Zurich, Switzerland
[c] Dept. Earth and Environmental Sciences, The University of Michigan, Ann Arbor, MI 48109, USA

ARTICLE INFO

Article history:
Received 20 July 2012
Received in revised form 15 May 2013
Accepted 17 May 2013
Available online 28 May 2013

Editor: U. Brand

Keywords:
Carbon sequestration
Serpentinization
Ocean Drilling Program
Northern Apennine
Iberian Margin
Ophiolites

ABSTRACT

Fluid circulation in peridotite-hosted hydrothermal systems influences the incorporation of carbon into the oceanic crust and its long-term storage. At low to moderate temperatures, serpentinization of peridotite produces alkaline fluids that are rich in CH_4 and H_2. Upon mixing with seawater, these fluids precipitate carbonate, forming an extensive network of calcite veins in the basement rocks, while H_2 and CH_4 serve as an energy source for microorganisms. Here, we analyzed the carbon geochemistry of two ancient peridotite-hosted hydrothermal systems: 1) ophiolites cropping out in the Northern Apennines, and 2) calcite-veined serpentinites from the Iberian Margin (Ocean Drilling Program (ODP) Legs 149 and 173), and compare them to active peridotite-hosted hydrothermal systems such as the Lost City hydrothermal field (LCHF) on the Atlantis Massif near the Mid-Atlantic Ridge (MAR).

Our results show that large amounts of carbonate are formed during serpentinization of mantle rocks exposed on the seafloor (up to 9.6 wt.% C in ophicalcites) and that carbon incorporation decreases with depth. In the Northern Apennine serpentinites, serpentinization temperatures decrease from 240 °C to <150 °C, while carbonates are formed at temperatures decreasing from ~150 °C to <50 °C. At the Iberian Margin both carbonate formation and serpentinization temperatures are lower than in the Northern Apennines with serpentinization starting at ~150 °C, followed by clay alteration at <100 °C and carbonate formation at <19–44 °C. Comparison with various active peridotite-hosted hydrothermal systems on the MAR shows that the serpentinites from the Northern Apennines record a thermal evolution similar to that of the basement of the LCHF and that tectonic activity on the Jurassic seafloor, comparable to the present-day processes leading to oceanic core complexes, probably led to formation of fractures and faults, which promoted fluid circulation to greater depth and cooling of the mantle rocks. Thus, our study provides further evidence that the Northern Apennine serpentinites host a paleo-stockwork of a hydrothermal system similar to the basement of the LCHF. Furthermore, we argue that the extent of carbonate uptake is mainly controlled by the presence of fluid pathways. Low serpentinization temperatures promote microbial activity, which leads to enhanced biomass formation and the storage of organic carbon. Organic carbon becomes dominant with increasing depth and is the principal carbon phase at more than 50–100 m depth of the serpentinite basement at the Iberian Margin. We estimate that annually 1.1 to 2.7×10^{12} g C is stored within peridotites exposed to seawater, of which 30–40% is fixed within the uppermost 20–50 m mainly as carbonate. Additionally, we conclude that alteration of oceanic lithosphere is an important factor in the long-term global carbon cycle, having the potential to store carbon for millions of years.

1. Introduction

Interaction of seawater with ultramafic rocks exposed at the ocean floor results in serpentinization reactions and the formation of hydrogen- and methane-rich fluids that can have a range of pH (2 to 11) and be highly alkaline at moderate to low temperature (Charlou et al., 1998, 2002; Kelley et al., 2001, 2005; Allen and Seyfried, 2003; Proskurowski et al., 2006). In contrast, some peridotite-hosted hydrothermal systems, such as the Rainbow and Logatchev hydrothermal fields, show evidence for input from interaction of seawater with mafic rocks, which is characterized by acidic and metal-rich fluids that discharge at high temperatures (e.g. Douville et al., 2002; Lackschewitz et al., 2005). Mixing of Ca-rich, alkaline fluids with seawater causes precipitation of carbonates within the oceanic lithosphere. At the peridotite-hosted Lost City hydrothermal field (LCHF), along the Mid-Atlantic Ridge (MAR), low-temperature (<40 to ~90 °C), high pH (9–11) fluids issue from carbonate-brucite structures and are diffusively

* Corresponding author. Tel.: +1 540 231 8521; fax: +1 540 231 3386.
E-mail address: esther11@vt.edu (E.M. Schwarzenbach).
[1] Present address: Virginia Tech Geosciences, 4044 Derring Hall, Blacksburg, VA 24061, USA.

0009-2541/$ – see front matter © 2013 Elsevier B.V. All rights reserved.
http://dx.doi.org/10.1016/j.chemgeo.2013.05.016

venting from the serpentinite basement causing extensive precipitation of carbonates (Kelley et al., 2001, 2005; Früh-Green et al., 2003; Ludwig et al., 2006; Proskurowski et al., 2008). Moreover, carbon geochemical studies by Delacour et al. (2008) on the serpentinite basement of the LCHF showed that extensive fluid circulation through the oceanic crust may lead to incorporation of dissolved organic carbon (DOC) from seawater within the serpentinites. Methane and hydrogen are considered to be major energy sources to sustain microorganisms in the subsurface of such hydrothermal systems (Kelley et al., 2005; Konn et al., 2009), while sulfur-oxidizing and sulfate-reducing bacteria as well as methane-metabolizing *Archaea* were found to inhabit the hydrothermal structures of the LCHF (Schrenk et al., 2004; Brazelton et al., 2006, 2010, 2011). Systems hosted by ultramafic rocks therefore not only play a major role in the cycling of abiogenic carbon but also support a unique microbiological system that is also of major importance in the study of the origin of life on Earth and other planets (McCollom, 1999, 2007; Schulte et al., 2006; Martin and Russell, 2007). Additionally, climate change and the concern for rising CO_2-concentrations in the atmosphere have stimulated interest in understanding CO_2 sequestration in ultramafic rocks through the carbonation of peridotite or serpentinite (e.g. Cipolli et al., 2004; Andreani et al., 2008; Kelemen and Matter, 2008; Matter and Kelemen, 2009; Klein and Garrido, 2011).

Many studies have discussed the process of serpentinization along mid-ocean ridges (e.g. Kelley et al., 2001; Mével, 2003; Bach et al., 2004; Früh-Green et al., 2004; Andreani et al., 2007), where tectonic activity leads to the exposure of ultramafic rocks at the seafloor inducing serpentinization at a wide range of temperatures ranging from less than 150 °C at the Iberian Margin (Agrinier et al., 1996) to 400–500 °C at the East Pacific Rise and Hess Deep (e.g. Bideau et al., 1991; Früh-Green et al., 1996).

Ophiolite complexes commonly comprise serpentinite sections rich in carbonate veins, carbonate-serpentine breccias and serpentine-hosted carbonate deposits, all of which are referred to as ophicalcites. Various ophicalcites are found in the Alpine orogenic belt and were formed in the Tethys ocean during the Mesozoic (e.g. Barbieri et al., 1979; Lemoine, 1980; Weissert and Bernoulli, 1985; Früh-Green et al., 1990; Desmurs et al., 2001). But many ophicalcite occurrences also date back as far as the Proterozoic and even the Archean (e.g. de Wit et al., 1987; Lavoie and Cousineau, 1995; Surour and Arafa, 1997). Similar carbonate precipitates and fracture-filling relationships in serpentinites have also been recovered through drilling into peridotite sections at the ocean–continent transition of the passive Iberian Margin (e.g. Gibson et al., 1996; Whitmarsh et al., 1998; Wilson, 2001; Hopkinson et al., 2004). These ophicalcites are similar to the stockwork system observed in the basement of the LCHF (Kelley et al., 2005; Ludwig et al., 2006), hence, they were likely also formed during low to moderate temperature hydrothermal and tectonic processes in near-ridge or fracture zone environments or during exhumation of subcontinental mantle along passive margins. Although the transient physico-chemical conditions associated with formation of these ancient deposits are commonly obscured by later recrystallization and metamorphic overprinting, outcrop studies of ancient ophicalcites offer important information on the geometry of fracture networks and fluid pathways. Geochemical studies, in addition, provide information for evaluating the importance of serpentinites as long-term sinks for seawater-derived elements (i.e., C, S, B, H_2O, Mg; Früh-Green et al., 2004; Boschi et al., 2008) including organic carbon and inorganic carbon (Delacour et al., 2008).

Here, we present a study of the carbon geochemistry of the Jurassic ophicalcites of the Northern Appenine ophiolites of Levanto (Italy) and of Cretaceous carbonate-veined serpentinites from the Iberian Margin (Ocean Drilling Program (ODP) Legs 149 and 173). Carbon contents and stable isotope compositions of organic carbon and inorganic carbon were analyzed to investigate the speciation and sources of carbon in these ancient hydrothermal systems and to investigate carbon storage over long geological time scales. Additionally, oxygen isotope measurements are used to estimate temperatures of water–rock interaction. Temperatures of serpentinization are likely controlled by the tectonic setting and may influence microbial activity. Thus, our results provide constraints on the thermal evolution of these systems and the extent of carbon sequestered during serpentinization with possible inputs from microbial activity.

2. Sampling and geological background

2.1. The Iberian Margin

The Iberian Margin (Fig. 1) is a Cretaceous non-volcanic, rifted continental margin formed during the opening of the North Atlantic through several phases of lithospheric extension and rifting (Sawyer et al., 1994). Along the western side of the ocean–continent transition (OCT) zone, mantle rocks were exposed to seawater leading to extensive serpentinization of a peridotite ridge and to the formation of a carbonate-vein network (Whitmarsh and Sawyer, 1996). The serpentinites from the Iberian Margin (Fig. 1) were drilled during three ODP cruises: Legs 103, 149 and 173. Serpentinized peridotite was recovered at 2 sites during Leg 149 (Sites 897 and 899). Site 897 is situated above the peridotite ridge at the edge of the OCT and Site 899 is located on an isolated basement high within the OCT (Sawyer et al., 1994). During Leg 173, serpentinites were drilled at Site 1070, which is located over an elongated basement ridge 20 km west of the peridotite ridge, and at Site 1068 near the southern edge of the Iberia Abyssal Plain (Whitmarsh et al., 1998). Analyses were conducted on 20 samples from Hole 897C, 29 samples from Hole 897D and 8 samples from Hole 899B. From Leg 173, 10 samples from the serpentinite basement of Hole 1070A and 3 serpentinite clasts of a breccia overlying this basement were analyzed.

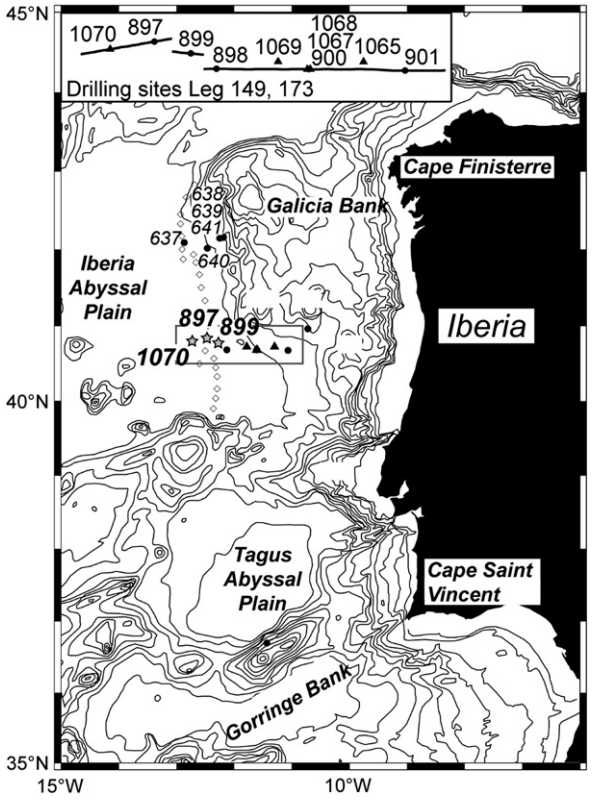

Fig. 1. Map of the Iberian Margin with the locations of the drill sites from the Ocean Drilling Program (ODP Legs 103, 149, and 173). The gray stars represent drill sites 897, 899 and 1070 that were analyzed in this study. Inset at the top is an enlargement of the gray rectangle in the map, showing the drill sites of ODP Legs 149 and 173. After Whitmarsh et al. (1998).

2.2. The Northern Apennine ophiolite

Ophiolite sequences exposed in the Northern Apennines are considered to have been formed in a mid-ocean ridge setting in the Ligurian Tethys as a result of the divergence of the European and Adriatic plates in the Middle Jurassic approximately 170 Ma ago (Barbieri et al., 1979; Abbate et al., 1980; Lemoine et al., 1987). Extension of the lithosphere and formation of a non-volcanic, passive margin were accompanied by the development of detachment faults (Marroni and Pandolfi, 2007). Exhumation of large amounts of sub-continental mantle along the detachment faults led to exposure of mantle rocks and consequently to extensive serpentinization already in the early stages in the opening of the Tethys Ocean (e.g. Rampone and Piccardo, 2000; Whitmarsh et al., 2001). After steady state seafloor spreading was established, the Ligurian Tethys probably comprised a slow-spreading ridge similar to the Mid-Atlantic Ridge, where further mantle exposure likely occurred along faults and at intersections with transform faults (Abbate et al., 1980, 1994; Lagabrielle and Cannat, 1990).

The sequences outcropping in the N. Apennines (Fig. 2) differ from classical ophiolite sequences in that they are usually missing the sheeted dike complex and are dominated by variably altered peridotite and gabbroic rocks with minimal amounts of basaltic lavas. In Liguria the serpentinites occur as the basement of the ophiolitic sequence and contain various amounts of calcite veins. Calcite-veining and oxidation

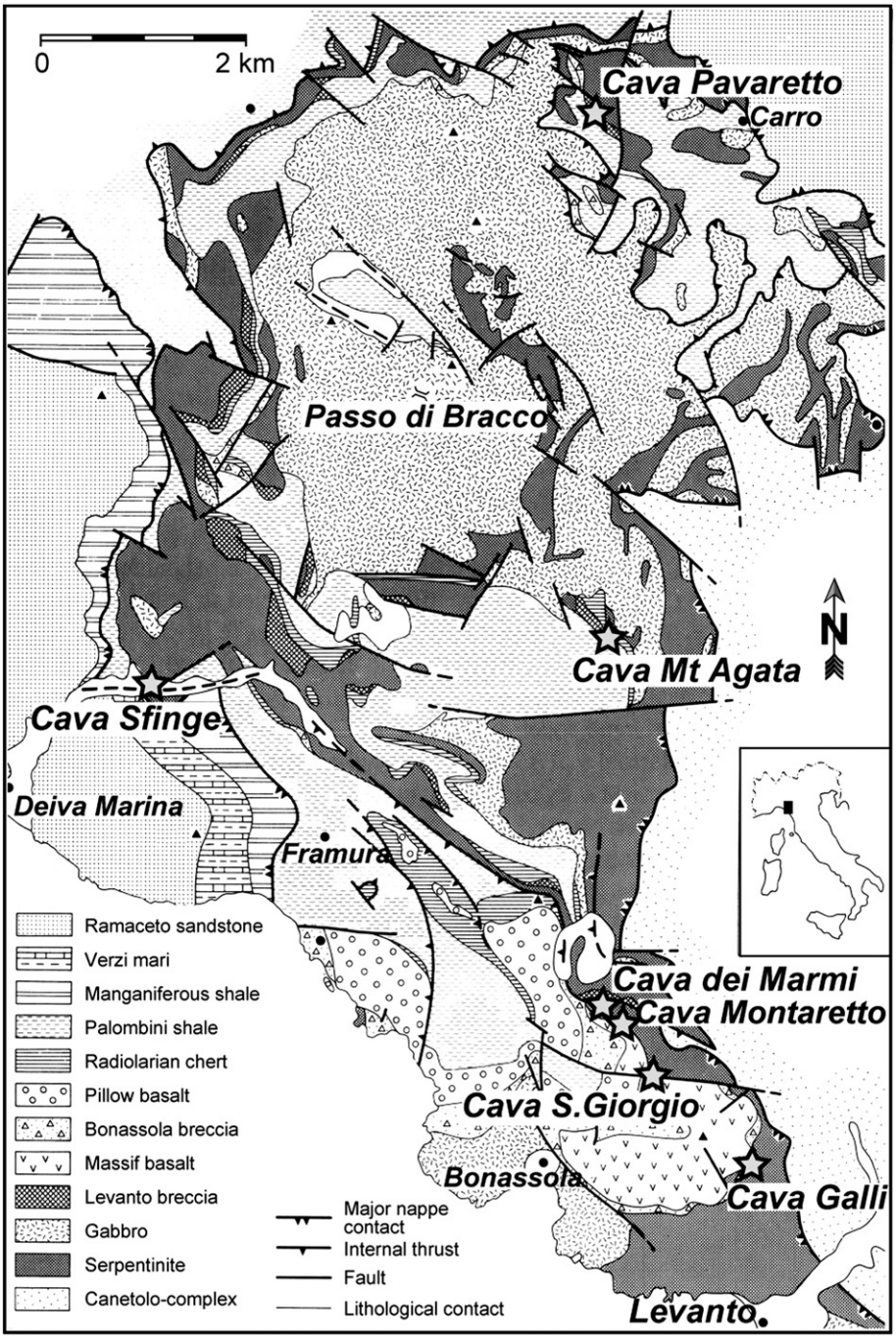

Fig. 2. Geological map of the Northern Apennine ophiolites, Liguria. After Strating (1991). Gray stars mark the location of the sampled quarries: Cava Galli, Cava San Giorgio, Cava Montaretto, Cava dei Marmi, Cava Sfinge, Cava Mt. Agata and Cava Pavaretto.

strongly increase to the top (Fig. 3), where the serpentinites merge into the red, so-called Levanto breccia, which we refer to as ophicalcites and which are quarried for building stones in a number of areas near the village of Levanto (Treves and Harper, 1994). A sedimentary sequence (Framura breccia) with serpentinitic, gabbroic and basaltic clasts in a calcareous, micritic matrix overlies the ophicalcites, and radiolarian cherts mark the top of the sequence (Cortesogno et al., 1980; Treves and Harper, 1994). Gabbros are mainly exposed around the Passo di Bracco area and along the coast near Bonassola (Fig. 2), while basaltic flows are rare and discontinuous (Cortesogno, 1981; Cortesogno et al., 1987; Molli, 1995). For our study, serpentinites and ophicalcites were collected in several quarries northwest of Levanto (Fig. 2).

3. Analytical methods

3.1. Carbon content and carbon isotope compositions

Our investigation is a collaborative study between the ETH Zurich and the University of Michigan. To examine the relationships between different veins and between the veins and the matrix, calcite veins were carefully isolated from the serpentinites and ophicalcites from the N. Apennines; matrix material was separated from major calcite veins, and bulk rock powder samples were prepared. On the serpentinites and ophicalcites from both the N. Apennines and the Iberian Margin, total carbon (TC) contents, total inorganic carbon (TIC) contents, $\delta^{13}C$ and $\delta^{18}O$ of the inorganic carbon, as well as $\delta^{13}C$ of the total carbon ($\delta^{13}C_{TC}$) and the total organic carbon ($\delta^{13}C_{TOC}$) were measured on bulk rock samples. In Table 3, samples marked with ($^{+}$) were measured at ETH Zurich. Samples marked with (*) were measured in Ann Arbor at the University of Michigan, where TIC contents were calculated as the difference between total carbon (TC) and total organic carbon (TOC). TIC can be considered to represent the carbonate content of the samples and in most samples from the Iberian Margin and from the N. Apennines is dominated by calcite (Plas, 1997; Schwarzenbach, 2011). Here we assume that the non-carbonate carbon represents total organic carbon (TOC), since no graphite could be detected in any of the analyzed samples. Carbon analyses in both laboratories were standardized relative to international standards.

3.1.1. Carbon analyses at ETH Zurich

Bulk rock powders were prepared by removing the outermost 2 cm from the rock with a diamond saw. In a hydraulic press the rock samples were crushed into <1 cm sized gravel, which was subsequently ground in an agate mill for 2 times 4 min. TC contents were measured at the Geological Institute on a CM 5012 CO_2 coulometer, where bulk rock powder was filled into tin capsules and combusted at 950 °C. To ensure that all of the carbon is oxidized to CO_2, oxygen carries the gas-products from the combustion zone through a barium chromate catalyst/scrubber to the CO_2 coulometer. TIC contents were measured on the same CO_2 coulometer, but in combination with a CM 5130 Acidification Module. Rock powder was filled in glass capsules and reacted with 2 molar perchloric acid, thereby releasing the carbonate as CO_2. To calculate TIC contents, we assumed that the carbonate was only present either as calcite or as aragonite, which was also confirmed by XRD-analysis. Precision for the coulometric measurements of the inorganic carbon is strongly dependent on the TIC content and was determined from laboratory internal standards and duplicate analyses to account for heterogeneity of the samples. Reproducibility for TIC is better than 2.5% for standards with more than 1 wt.% C and maximum error for samples with <600 ppm C is ±50 ppm. Reproducibility of the TC measurements is better than 1% for standards with more than 1 wt.% C, and maximum error at <600 ppm C is ±30 ppm. Total organic carbon (TOC) contents were calculated as the difference from the TC and TIC measurements.

The $\delta^{13}C_{TC}$ and $\delta^{13}C_{TOC}$ measurements were carried out on a Thermo Scientific Flash Elemental Analyzer (EA) (1112 Series) interfaced with a Conflo IV to a Delta V Plus Isotope Ratio Mass Spectrometer (MS). Bulk rock powders were analyzed for $\delta^{13}C_{TC}$. For $\delta^{13}C$ of the organic carbon, bulk rock samples were reacted with 3 N HCl to remove all acid-soluble carbon, washed with distilled H_2O and dried at 60 °C

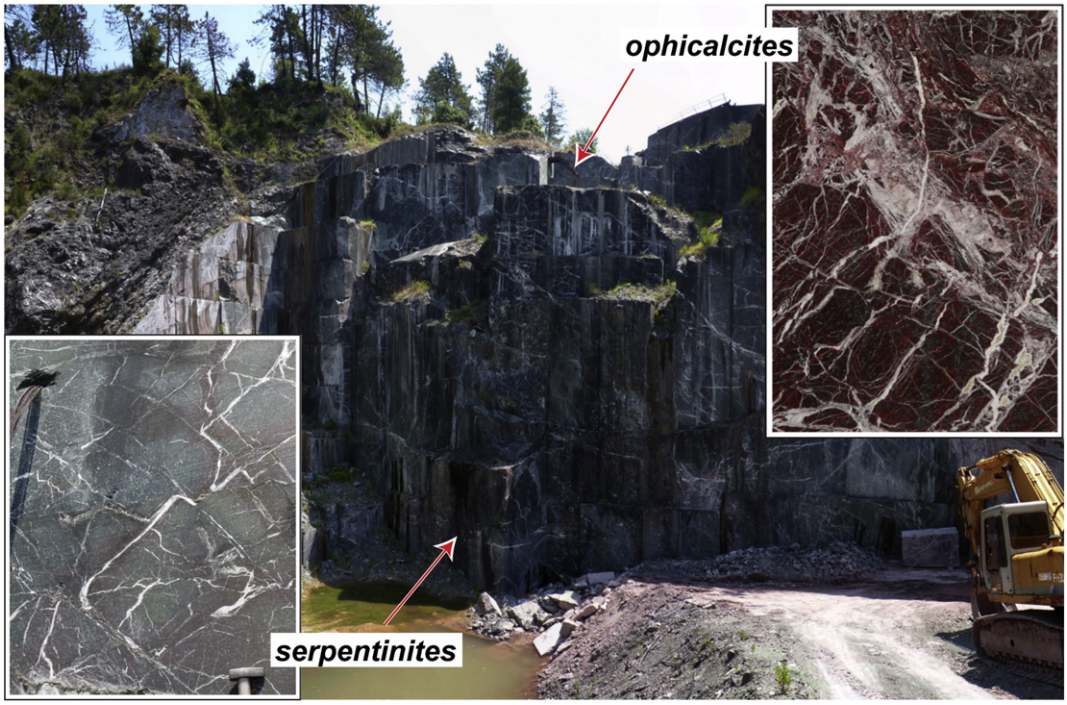

Fig. 3. Cava dei Marmi northwest of Levanto. The basement of the ophiolite sequence comprises of variably calcite-veined serpentinites, which merge towards the top of the sequence into strongly calcite- and serpentine-veined and oxidized, red ophicalcites. The serpentinites and ophicalcites are exposed over a height of approximately 30 m.

over night. The remaining powder was homogenized by hand in an agate mortar before analyses on the Flash EA. To ensure accuracy of the measurements we used internal laboratory standards calibrated to NBS 22 ($\delta^{13}C = -30.03‰$) yielding a reproducibility better than 0.5% (2σ). Carbon isotope values are reported in the conventional δ-notation with respect to the Vienna Pee Dee Belemnite (VPDB) standard.

Calcite veins from bulk rocks and a subset of bulk rock samples were analyzed for $\delta^{13}C$ and $\delta^{18}O$ of the TIC either on a Thermo Fisher Scientific Kiel IV carbonate device coupled to a MAT253 mass spectrometer or on a Finnigan GasBench II interfaced with a Conflo IV to a Delta V Plus Isotope Ratio MS at the Geological Institute at ETH Zurich. The $\delta^{18}O$ values of calcite on the VPDB scale were converted to the Vienna Standard Mean Ocean Water standard (VSMOW) using the equation of Coplen et al. (1983): $\delta^{18}O_{VSMOW} = 1.03091 * \delta^{18}O_{VPDB} + 30.91$. Analytical reproducibility was better than ±0.07‰ and ±0.15‰ for $\delta^{13}C$ and $\delta^{18}O$ respectively.

3.1.2. Carbon analyses at Ann Arbor

Contents and isotope compositions of TC and TOC were determined by elemental analyzer. Inorganic carbon was removed by reaction with 3 N HCl, followed by washing with distilled H_2O. The $\delta^{13}C$ of TC and TOC was determined at the University of Michigan, using a Costech element analyzer coupled to a Thermo Scientific Delta V plus mass spectrometer. Carbon contents were calibrated using a range of masses of Acetanilide (71.09 wt.% C) and calibration standards for carbon isotopes were IAEA 600 Caffeine ($\delta^{13}C = -27.77‰$) and IAEA-CH-6 Sucrose (−10.45‰). To minimize adsorption of atmospheric CO_2, powders were degassed at 100 °C and stored under vacuum in a desiccator. At high carbon concentrations (>0.1 wt.%) reproducibility is better than 2% of reported values, but the maximum error at low-carbon contents (<500 ppm C) is ±70 ppm, similar in absolute error but a greater proportion of the reported carbon content. Uncertainties in $\delta^{13}C$ are ±0.5‰, and carbon blanks are less than 6% of reported carbon contents (<0.0024 wt.% C with $\delta^{13}C$ values of blanks = −22 to −29‰) and thus contribution of carbon blanks is insignificant.

3.2. Isotope analyses of serpentine, magnetite and bulk rocks

Oxygen and hydrogen isotope analyses were performed on serpentine mineral separates and separated serpentine veins on selected samples from Leg 149. Due to very fine-grained intergrowths of magnetite with serpentine, only one serpentine–magnetite pair was determined on sample 149-47 from Leg 149 to calculate serpentinization temperatures. Additionally, bulk rock oxygen isotope analyses were performed on selected samples from the N. Apennine serpentinites.

For mineral separation, crushed bulk rocks and drilled serpentine veins were sieved at different grain sizes, washed in HCl to remove calcite impurities and cleaned with distilled water in an ultrasonic bath. Magnetite was removed by use of a hand-magnet. Treatment in a standard high-density liquid of suitable size fraction (generally 88 to 125 μm or 125 to 177 μm) allowed the separation of serpentine, amphibole, olivine and talc. Magnetite was separated in a high-density liquid column using the different sedimentation velocities. Small amounts of impurities for all samples were finally eliminated by hand picking under the binocular microscope. Sample purity was better than 95%.

Oxygen isotope ratio analyses of serpentine in the Leg 149 samples (Table 1) were performed by conventional fluorination with ClF_3 in nickel-reaction vessels at temperatures of 600–650 °C (Borthwick and Harmon, 1982). Oxygen was converted to carbon dioxide by oxidation of heated carbon. Oxygen isotope compositions of CO_2 were then determined on a VG OPTIMA dual inlet mass spectrometer at the ETH Zurich. Delta values were calibrated with the international NBS 28 quartz standard with a $\delta^{18}O$ value of 9.6‰. Repeat measurements yielded a 1σ standard deviation of ±0.25‰.

Analysis of the oxygen isotope ratio of magnetite was performed at the laser extraction line of the stable isotope laboratory of the University of Lausanne. The sample was heated by a CO_2 laser beam and reacted in a BrF_5 atmosphere. The oxygen was transferred to a combustion chamber through a mercury diffusion pump and converted to CO_2 by oxidation of heated carbon. Isotopic composition was determined on a FINNIGAN MAT251 dual inlet mass spectrometer with a reproducibility of ±0.2‰.

For hydrogen isotope ratio analyses of serpentine 20 to 30 mg of mineral separate was dried overnight at 150–200 °C. The samples were then dehydrated in vacuum at temperatures >1000 °C. Molecular hydrogen was converted to H_2O in a copper oxide bypass. The resulting total water was quantitatively converted to H_2 by oxidation of elemental zinc at 500 °C. Hydrogen isotope compositions were measured on a VG OPTIMA dual inlet mass spectrometer. An internal laboratory standard of antigorite, calibrated against the international NBS30 biotite standard with a value of −65‰, was used to determine δD-values, and repeated sample measurements yielded a reproducibility of better than ±2‰.

Oxygen isotope analyses of serpentinites from the N. Apennines (Table 3) were carried out at the University of Michigan. Bulk rock sample powders were first reacted with 3 N HCl to remove acid soluble carbonate. The samples were then reacted with BrF_5 in externally heated nickel reaction vessels (Clayton and Mayeda, 1963). The liberated O_2 was converted to CO_2 gas by reaction with heated carbon rods. Oxygen isotope ratios were measured using a Finnigan Delta-S mass spectrometer. All samples were run in duplicate and analyses were calibrated with NBS 28 quartz. Repeat measurements yielded a precision of ±0.5‰.

4. Results

4.1. Carbon geochemistry

4.1.1. The Iberian Margin

The serpentinites from the Iberian Margin show strong variations in total carbon (TC) contents, which are mainly dependent on the amount of inorganic carbon (TIC). The highest concentrations are observed at the top of the basement close to the transition to the sediments, where TIC contents reach up to 9.6 wt.% (Hole 897C, sample 149-21; Table 1). The TIC contents decrease strongly downhole, with the largest changes associated with shear zones (Sawyer et al., 1994). TIC contents are <0.1 wt.% below ~680 meter below seafloor (mbsf) in Hole 897C and below ~770 mbsf in Hole 897D (Fig. 4). The $\delta^{13}C_{TC}$ decreases downward, from values of −2 to +2‰ at the top (above ~670 mbsf at Hole 897C and above ~760 mbsf at Hole 897D) to values as low as −23.1‰ at Hole 897C (at ~680 mbsf) and −25.3‰ at Hole 897D (at ~820 mbsf). This trend reflects a change in carbon speciation from dominantly carbonate at the top to mainly organic carbon immediately below the major shear zones. $\delta^{13}C_{TC}$ values become less negative again towards the bottom of Holes 897C ($\delta^{13}C_{TC} = -4.3‰$) and 897D ($\delta^{13}C_{TC} = -8.7‰$). At Hole 897C, the trend to higher $\delta^{13}C_{TC}$ values is accompanied by slightly heavier organic carbon with $\delta^{13}C_{TOC}$ values up to −22.9‰ (at ~740 mbsf). In Hole 897D, TOC contents are slightly higher in the lower part than in the upper part of the hole, while in Hole 897C the highest TOC contents are found directly at or above a zone of sheared breccias and serpentinites (Fig. 4). The carbonate veins have a range in $\delta^{13}C_{TIC}$ of −1.7 to +1.8‰.

Serpentinites of Leg 173 yielded TOC contents of <200 ppm (Table 2). TC and TIC contents in the serpentinite basement are generally <0.1 wt.% with the exception of one sample at the top of the sequence close to the transition to the breccias, which has a slightly higher TC content due to intense carbonate-veining. $\delta^{13}C_{TC}$ values are between −9.5 and −5.6‰ and $\delta^{13}C_{TOC}$ values are between −26.7 and −23.0‰.

Table 1
Carbon content and carbon isotope composition on total carbon (TC), total inorganic carbon (TIC), and total organic carbon (TOC), and oxygen and hydrogen isotope compositions from serpentine mineral separates, and carbon and oxygen isotope composition on calcite and serpentine veins from the Iberian Margin, ODP Leg 149.

Sample	Hole	Depth (mbsf)	Lith. [a]	TC (%C)	TIC (%C)	TOC (ppm)	$\delta^{13}C_{TC}$ (‰)	$\delta^{13}C_{TIC}$ (‰)	$\delta^{18}O_{TIC}$ (‰) (VSMOW)	$\delta^{13}C_{TOC}$ (‰)	T (°C)[b]	$\delta^{18}O_{serp}$ (‰) [c]	δD serp (‰) [c]	$\delta^{18}O_{serp\ vein}$ (‰)	$\delta D_{serp\ vein}$ (‰)	$\delta^{13}C$ (‰) cc vein A [e]	$\delta^{18}O$ (‰) (VSMOW) cc vein A [e]	T (°C) vein A[b], [e]	$\delta^{13}C$ (‰) cc vein B [e]	$\delta^{18}O$ (‰) (VSMOW) cc vein B [e]	T (°C) vein B[b], [e]
149_01	897C	650.77	PE	3.501	3.438	630	−2.5	−0.4	30.9	−27.6	20	6.0	−69.3								
149_02	897C	661.17	PE	1.304	1.241	623	−1.0	0.8	30.6	−26.8	21					1.3	31.0	20			
149_03	897C	661.72	PE	1.190	1.145	445	−1.4	0.4	31.0	−26.8	20					0.6	30.5	22	0.1	30.7	21
149_04	897C	662.49	PE	6.182	6.140	420	−1.0	0.6	30.7	−27.4	21	2.8	−65.6								
149_05	897C	662.79	PE	3.920	3.729	1913	−2.1	0.6	31.0	−28.0	20	[d] 11.3‡	−69.0								
149_06	897C	668.30	PE													0.8	29.5	27			
149_07	897C	670.21	PE	2.409	2.113	2963	−3.8	0.8	30.4	−27.0	23	7.4	−70.8			0.7	30.4	22			
149_08	897C	671.08	PE	8.463	7.763	7000	−0.2	1.7	31.0	−28.3	20					1.5	30.4	22			
149_09	897C	677.80	PE	0.295	0.050	2442	−20.2	<l.o.d.	<l.o.d.	−27.6		5.9	−71.5								
149_10	897C	680.92	PE	0.085	0.028	603	−21.1	<l.o.d.	<l.o.d.	−26.0											
149_11	897C	681.38	PR	0.047	0.020	300	−23.1	<l.o.d.	<l.o.d.	−27.2											
149_12	897C	687.03	PE	0.065	0.023	458	−19.4	<l.o.d.	<l.o.d.	−27.1											
149_13	897C	688.52	PE																		
149_14	897C	689.84	PE	0.040	0.014	264	−21.1	<l.o.d.	<l.o.d.	−27.5											
149_15	897C	707.10	PE	0.152	0.012	1401	−21.3	<l.o.d.	<l.o.d.	−27.5		6.8	−74.7								
149_16	897C	711.40	PR	0.142	0.040	1021	−18.9	<l.o.d.	<l.o.d.	−27.5				11.8	−79.0						
149_17	897C	713.25	DU	0.135	0.023	1125	−19.7	<l.o.d.	<l.o.d.	−27.3		5.3	−66.0								
149_18	897C	718.70	PE	0.083	0.030	534	−18.9	<l.o.d.	<l.o.d.	−27.3		5.8	−71.6								
149_56	897C	726.34	PE	0.135	0.108	270	−4.3	<l.o.d.	<l.o.d.	−23.3											
149_57	897C	737.21	PE	0.135	0.115	200	−4.3	<l.o.d.	<l.o.d.	−22.9											
149_58	897C	738.41	PE	0.106	0.086	204	−5.7	<l.o.d.	<l.o.d.	−26.4											
149_19	897D	686.37	PE	1.905	1.771	1345	−2.6	0.1	29.7	−27.3	26	7.7	−73.5								
149_20	897D	698.65	PE	6.191	6.196	<l.o.d.	−0.1	1.1	31.2	−26.6	19					0.6	30.9	20			
149_21	897D	705.75	PE	9.629	9.615	137	1.3	2.3	31.1	−26.8	19					1.8	30.6	22			
149_22	897D	713.85	PE	4.469	4.437	322	−0.9	0.5	30.8	−25.3	21					0.5	31.0	20	0.2	31.2	19
149_23	897D	718.92	PE	3.262	3.206	557	−1.0	0.6	29.5	−25.1	26								0.3	30.5	22
149_24	897D	743.11	PE	4.474	4.414	605	−2.0	−0.3	30.8	−27.6	21								0.3	30.8	21
149_25	897D	743.38	PE	1.249	1.208	415	−4.3	−1.5	29.7	−27.1	26					−1.7	30.4	23			
149_26	897D	743.96	PE	2.684	2.633	508	−1.7	−0.2	30.0	−26.5	24								−0.3	30.3	23
149_27	897D	748.52	PE	6.604	6.545	590	0.4	1.9	30.4	−26.3	23										
149_28	897D	751.93	PE	6.768	6.749	195	0.6	1.9	30.0	−26.3	24										
149_29	897D	752.02	PE	7.289	7.291	<l.o.d.	0.6	1.9	29.9	−25.9	25					1.3	29.5	27			

149_30	897D	753.50	PE	5.701	5.610	907	0.2	1.6	29.6	−26.3	26									
149_31	897D	754.80	PE	3.641	3.610	313	−1.0	1.2	28.6	−26.7	31					0.8	27.6	36	1.6	26.1	44
149_32	897D	756.37	PE	4.129	4.085	432	−0.5	1.1	29.8	−26.5	25									
149_33	897D	757.33	PE	3.365	3.142	2230	−1.3	0.3	29.7	−27.8	26	7.5	−73.9							
149_34	897D	758.40	PE	5.578	5.486	920	−1.5	−1.1	29.9	−27.0	25					−0.5	29.0	29	−0.6	29.4	27
149_35	897D	772.93	PE	0.218	0.015	2026	−22.2	<l.o.d.	<l.o.d.	−27.7										
149_36	897D	773.16	PE	0.326	0.011	3153	−24.0	<l.o.d.	<l.o.d.	−27.6										
149_37	897D	773.60	PE	0.065	0.010	558	−19.5	<l.o.d.	<l.o.d.	−28.2										
149_38	897D	775.50	PE	0.160	0.117	429	−12.6			−28.3				12.4	−58.0					
149_39	897D	776.73	PE	0.107	0.044	627	−16.0	<l.o.d.	<l.o.d.	−27.1				14.2	−77.0					
149_40	897D	782.77	PE	0.113	0.020	933	−20.1	<l.o.d.	<l.o.d.	−28.3										
149_41	897D	791.24	PE	0.462	0.038	4245	−24.0	<l.o.d.	<l.o.d.	−28.3		7.0	−66.9							
149_42	897D	801.12	PE	0.259	0.071	1876	−17.0	<l.o.d.	<l.o.d.	−27.2		6.1	−70.3							
149_43	897D	809.30	PE	0.320	0.120	2004	−18.6	<l.o.d.	<l.o.d.	−28.1				8.6	−74.0					
149_44	897D	814.73	PE	0.309	0.117	1918	−15.6	<l.o.d.	<l.o.d.	−28.1										
149_45	897D	819.51	PE	0.049	0.008	418	−25.3	<l.o.d.	<l.o.d.	−28.1										
149_46	897D	830.86	PE																	
149_59	897D	831.40	PE	0.033	0.028	47	−13.7	<l.o.d.	<l.o.d.	−24.9										
149_60	897D	834.55	PE	0.114	0.185	<l.o.d.	−8.7	<l.o.d.	<l.o.d.	−27.2										
149_47	899B	483.95	PE	0.192	0.048	1437	−16.7	<l.o.d.	<l.o.d.	−28.3		9.3	−66.4							
149_48	899B	502.38	PE	0.074	0.005	688	−21.1	<l.o.d.	<l.o.d.	−27.9										
149_49	899B	502.99	PE	0.823	0.580	2435	−7.1	−2.0	31.0	−28.2	20	3.1‡	−68.5							
149_50	899B	510.60	BA	0.123	0.014	1092	−21.0	<l.o.d.	<l.o.d.	−27.9		[d)] 12.8	−64.9							
149_51	899B	511.60	PE	0.167	0.020	1472	−16.9	<l.o.d.	<l.o.d.	−27.9										
149_52	899B	512.01	PE	0.705	0.615	900	−5.2	−1.1	30.1	−28.2	24			3.8	−63.0					
149_53	899B	529.75	DIA									[d)] 13.2‡	−48.4							
149_54	899B	539.20	GA	0.058	0.003	544	−17.7	<l.o.d.	<l.o.d.	−28.1										
149_55	899B	548.58	GA	0.433	0.377	560	−3.8	−1.1	26.8	−28.2	40									

<l.o.d. = below limit of detection

[a] DU—dunite;GA — gabbro; PE — peridotite; DIA—diabase; PR—pyroxenite; BA—basalt.

[b] Temperature calculated using the equation:$1000\ln\alpha = 2.78(10^6 * T^{-2}) - 2.89$ from Friedman and O'Neil (1977).

[c] $\delta^{18}O$ values from serpentine separates;‡ = the indicated value represents the average ratio of two measurements on the same sample.

[d] Not pure serpentine separates that contain clay.

[e] Veins A and B are separated calcite veins from serpentinite bulk rocks.

A) ***Leg 149, Hole 897C***

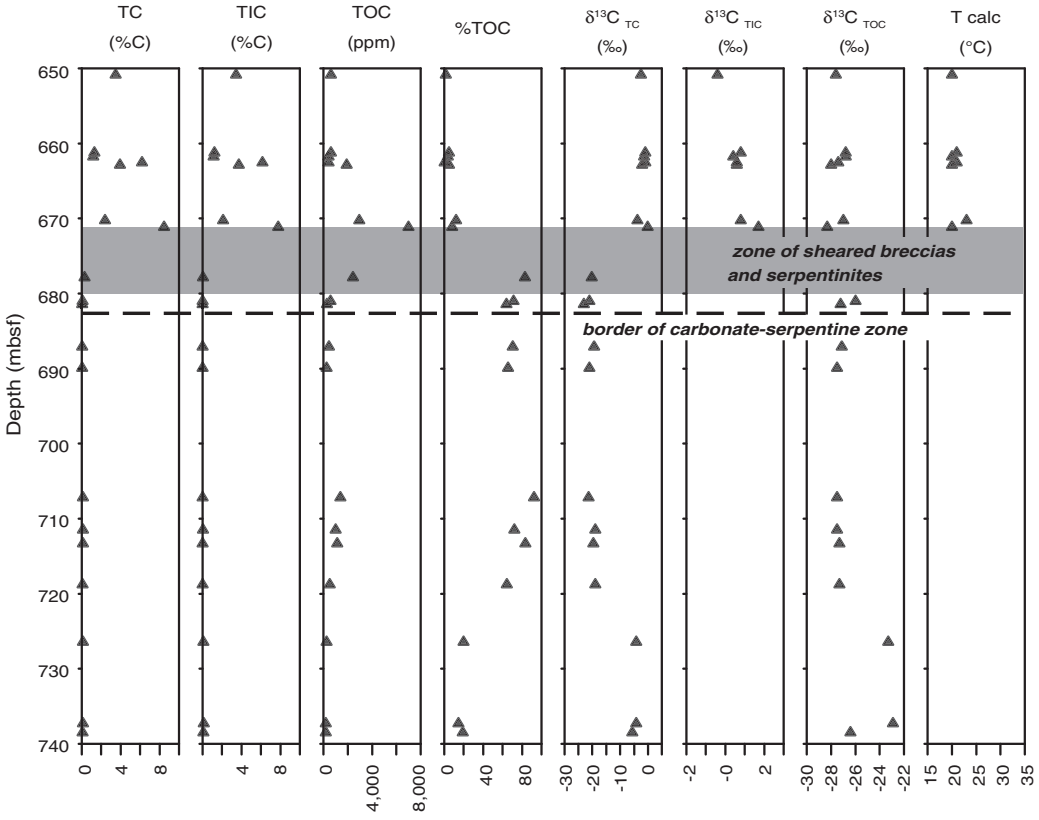

B) ***Leg 149, Hole 897D***

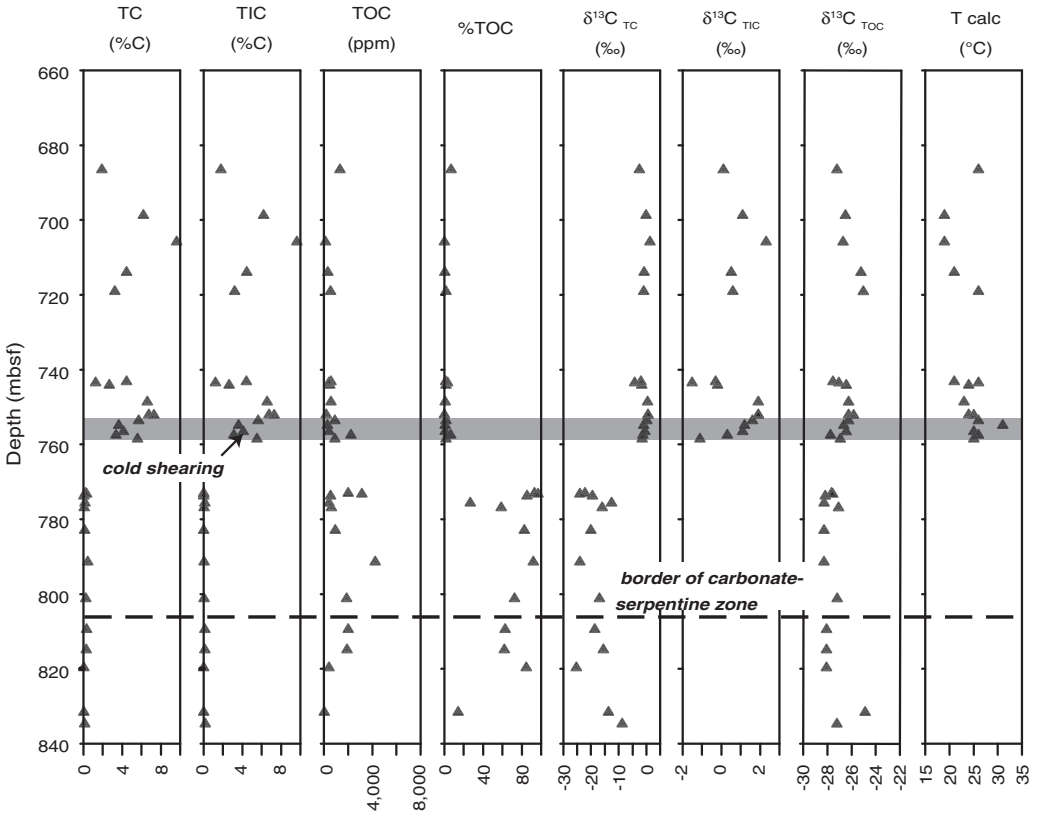

Table 2
Carbon content and carbon isotope composition on total carbon (TC), total inorganic carbon (TIC), and total organic carbon (TOC) from the Iberian Margin, ODP Leg 173.

Sample	Hole	Depth (mbsf)	Lith. [a)]	TC (%C)	TIC (%C)	TOC (ppm)	$\delta^{13}C$ TC (‰)	$\delta^{13}C$ TIC (‰)	$\delta^{18}O_{TIC}$ (‰) (VSMOW)	$\delta^{13}C_{TOC}$ (‰)	T (°C) [b)]
173_1	1070A	667.69	Clast	0.595	0.586	190	0.7	1.1	29.8	−24.8	21
173_2	1070A	668.91	Clast	1.997	2.010	<l.o.d.	1.4	1.6	30.4	−24.5	18
173_3	1070A	669.86	Clast	2.930	2.902	276	1.6	1.5	30.2	−25.4	19
173_4	1070A	686.38	PE								
173_5	1070A	696.36	PE	0.442	0.421	209	−5.9	−2.0	27.9	−25.4	29
173_6	1070A	696.74	PE	0.043	0.029	144	−9.5			−25.4	
173_7	1070A	705.47	PE	0.059	0.046	129	−7.0			−25.1	
173_8	1070A	706.34	PE	0.075	0.063	119	−6.8			−25.7	
173_9	1070A	706.98	PE	0.056	0.039	173	−6.7			−24.7	
173_10	1070A	708.78	PE	0.056	0.042	140	−7.0			−25.9	
173_11	1070A	710.91	PE	0.050	0.036	142	−8.2			−24.5	
173_12	1070A	714.84	PE	0.052	0.041	114	−5.6			−23.0	
173_13	1070A	717.73	PE	0.043	0.029	145	−8.2			−26.7	

[a)] PE — serpentinized peridotite; clast — serpentinite clast in the breccia.
[b)] Temperature calculated using the equation: $1000\ln\alpha = 2.78(10^6 * T^{-2}) - 2.89$ from Friedman and O'Neil (1977).

4.1.2. Serpentinites and ophicalcites from the Northern Apennine

Similar to the upper zones of the Iberian Margin basement, total carbon contents of the serpentinites from the N. Apennines show a dominance of inorganic carbon where high TC contents are observed (Table 3). This is reflected in the $\delta^{13}C_{TC}$ values, with high TC contents corresponding to $\delta^{13}C_{TC}$ of ~0‰, consistent with a marine carbonate signature, and very low TC contents being associated with negative $\delta^{13}C_{TC}$ values (Fig. 5), reflecting a dominance of organic carbon. TOC contents are considerably lower than at the Iberian Margin Site 897 and generally <400 ppm, except for one ophicalcite sample, which has an organic carbon content of >0.1 wt.%. $\delta^{13}C_{TOC}$ and $\delta^{13}C_{TIC}$ values show a range of −27.1 to −16.9‰ and −2.9 to +2.8‰, respectively.

4.2. Temperatures of calcite precipitation

The carbonate veins from the N. Apennines are dominated by calcite (Schwarzenbach, 2011) and at the Iberian Margin, the veins are calcite with traces of aragonite (Plas, 1997). Calcite-precipitation temperatures were calculated from oxygen isotope compositions using the calcite–water fraction factor given in Friedman and O'Neil (1977) and assuming a $\delta^{18}O_{Seawater\ (SMOW)} = 0$‰, similar to that used by Agrinier et al. (1996). With a value of $\delta^{18}O_{Seawater} = -1$‰, which is the average composition of the ocean for an ice-free world, the calculated temperatures would be approximately 8–9 °C lower.

At the Iberian Margin, calculated temperatures are between 19 and 44 °C. Due to very low carbonate contents in samples from Leg 173, the temperature of calcite precipitation could only be calculated for one sample from the basement and yielded 29 °C, while the overlying serpentinite clasts yielded temperatures of 18–21 °C (Table 2). Calculated temperatures of calcite precipitation are distinctly higher in the N. Apennine serpentinites and range between 49 and 151 °C (Fig. 6, Table 3). In addition, comparison between matrix and calcite veins, and between several generations of calcite veins, yielded differences in temperatures of up to 70 °C within individual samples (Fig. 7).

4.3. Oxygen and hydrogen isotope compositions of the Iberian Margin serpentinites

The $\delta^{18}O$ values of serpentines of the Iberian Margin are shown in Table 1. Pure serpentine separates yielded $\delta^{18}O$-values between 5.3 and 9.3‰. Samples 149-5, 149-50, and 149-53 contain vermiculite and have values of 11.3–13.2‰, and thus are clearly higher than the pure serpentine. Four late, white, thick crosscutting serpentine veins displaying very similar mineralogical and textural characteristics, and representing a unique generation, have $\delta^{18}O$-values of 8.6–14.2‰, and are distinctly higher than the pure matrix serpentines. Hydrogen isotope values of the serpentine separates range from −75 to −66‰, whereby one clay-containing sample has a δ_D-value of −48‰. These values lie within the range of compositions of serpentinites formed at ridge settings (e.g. Wenner and Taylor, 1973; Sakai et al., 1990; Agrinier et al., 1996; Früh-Green et al., 1996; Agrinier and Cannat, 1997).

Due to very fine-grained intergrowths of magnetite and serpentine, only one pure magnetite sample (from sample 149-47) could be measured and had a $\delta^{18}O$ of −0.8‰, yielding a calculated $\Delta_{serpentine-magnetite} = 10.1$‰. Empirical serpentine–magnetite and serpentine–water fractionation curves were proposed by Wenner and Taylor (1971, 1973) and were discussed by Früh-Green et al. (1996). Applying the three fractionation curves discussed by Früh-Green et al. (1996) we obtain the following range of equilibrium temperatures:

(1) $10^3\ln\alpha_{serpentine-magnetite} = 1.42 * 10^6/T^2 + 0.93$ $T = 120$ °C (Früh-Green et al., 1996)
(2) $10^3\ln\alpha_{serpentine-magnetite} = 1.81 * 10^6/T^2 + 1.41$ $T = 185$ °C (Früh-Green et al., 1996)
(3) $10^3\ln\alpha_{serpentine-magnetite} = 1.69 * 10^6/T^2 + 1.68$ $T = 175$°C (Wenner and Taylor, 1971).

Although there is a large uncertainty in the fractionation factors, all three curves suggest that serpentinization at the Iberian Margin occurred at temperatures less than 200 °C. This is consistent with data of two serpentine–magnetite pairs measured by Agrinier et al. (1996) in serpentinites from Leg 149, which yielded $\Delta_{serpentine-magnetite}$ of 11.0 and 12.5‰ respectively, and corresponds to even lower equilibrium temperatures.

4.4. Oxygen isotope composition of the Northern Apennine serpentinites

The bulk rock $\delta^{18}O$ values of the serpentinites from the N. Apennines are between 6.7 and 9.9‰ (Table 3). Samples from Cava dei Marmi and Cava Montaretto, which are within a few 100 m of each other, yield an

Fig. 4. Carbon geochemistry of the Iberian Margin, ODP Leg 149 Holes A) 897C and B) 897D, showing carbon contents and isotope compositions of total carbon (TC), total inorganic carbon (TIC), and total organic carbon (TOC), and %TOC of the total carbon with depth. Temperatures are calculated from $\delta^{18}O_{TIC}$ values after Friedman and O'Neil (1977). Dashed lines mark the border of the carbonate-serpentine zones as defined by Alt and Shanks (1998). At both Hole 897C and Hole 897D, strong changes in the carbon signatures occur where zones of intense shearing characterize the basement (gray bars). Locations of the shear zones are from Sawyer et al. (1994).

Table 3
Carbon content and carbon isotope composition on total carbon (TC), total inorganic carbon (TIC), and total organic carbon (TOC), and oxygen isotope composition from serpentinite bulk rocks from the Northern Apennine ophiolite.

Sample name [a)]	Location	Coordinates		Rock type [b)]	Analyzed part [c)]	TC (%C)	TIC (%C) [d)]	TOC (ppm)	δ^{13}C TC (‰)	δ^{13}C TIC (‰)	δ^{18}O TIC (‰) (VSMOW)	δ^{13}C TOC (‰)	T(°C) [e)]	$\delta^{18}O_{WR}$ (‰)
		N	E											
102408-1A*	Cava Galli	44°11′51.06″	009°35′20.7″	Unveined		0.071	*0.053*	180	−3.5			−22.0		
102408-3*	Cava Galli	44°11′51.06″	009°35′20.7″	dk serp		0.027	*0.013*	140	−11.1			−24.0		
LGA1+	Cava Galli	44°11′51.06″	009°35′20.7″	S	S (WR)	0.027	0.020	70	−6.8	<l.o.d.	<l.o.d.	−25.1		6.7
LGA3+	Cava Galli	44°11′51.06″	009°35′20.7″	S	S (WR)	0.020	0.010	103	−10.1	<l.o.d.	<l.o.d.	−25.2		
LGA3 Cc-A+	Cava Galli	44°11′51.06″	009°35′20.7″	S	CC (V)					1.1	13.5		140	
LGA3 Cc-B+	Cava Galli	44°11′51.06″	009°35′20.7″	S	CC (V)					1.4	12.7		151	
LGA4+	Cava Galli	44°11′51.06″	009°35′20.7″	CC	CC					1.2	12.7		150	
LGA6 Serp+	Cava Galli	44°11′51.06″	009°35′20.7″	O	O (WR)	1.177				1.6	14.7		126	
LGA6 Oph+	Cava Galli	44°11′51.06″	009°35′20.7″	O	O (M)	0.795	0.772	230	1.0	1.4	13.3	−25.5	142	
LGA6 Cc-A+	Cava Galli	44°11′51.06″	009°35′20.7″	O	CC (V)					1.6	16.2		110	
LGA6 Cc-B+	Cava Galli	44°11′51.06″	009°35′20.7″	O	CC (V)					2.2	17.9		94	
LGA6 Cc-C+	Cava Galli	44°11′51.06″	009°35′20.7″	O	CC (V)					1.8	20.7		72	
LGA8 Cc-A+	Cava Galli	44°11′51.06″	009°35′20.7″	O	CC (V)					1.2	14.8		125	
LGA8 Cc-B+	Cava Galli	44°11′51.06″	009°35′20.7″	O	CC (V)					1.4	14.6		127	
LGA8 Cc-C+	Cava Galli	44°11′51.06″	009°35′20.7″	O	CC (V)					2.5	18.9		86	
LGA8 Cc-D+	Cava Galli	44°11′51.06″	009°35′20.7″	O	CC (V)					0.5	17.2		101	
LMO1 Serp+	Cava Montaretto	44°11′46.44″	009°35′20.46″	S	S (WR)	3.252	3.246	55	1.1	1.8	16.3	−24.5	109	
LMO1Cc+	Cava Montaretto	44°11′46.44″	009°35′20.46″	S	CC (V)					2.6	18.0		93	
LMO2+	Cava Montaretto	44°11′46.44″	009°35′20.46″	S	S (WR)	0.873	0.858	155	0.6	0.8	15.2	−24.9	120	
LMO3 Cc-A+	Cava Montaretto	44°11′46.44″	009°35′20.46″	O	CC (V)					0.4	15.9		113	
LMO3 Cc-B+	Cava Montaretto	44°11′46.44″	009°35′20.46″	O	CC (V)					2.6	17.4		98	
LMO4+	Cava Montaretto	44°11′46.44″	009°35′20.46″	CC	CC					0.5	15.6		116	
LMO5-A+	Cava Montaretto	44°11′46.44″	009°35′20.46″	O	O (M)					2.4	15.7		114	
LMO5-B+	Cava Montaretto	44°11′46.44″	009°35′20.46″	O	O (M)					2.3	15.8		114	
LMO5 Cc-A+	Cava Montaretto	44°11′46.44″	009°35′20.46″	O	CC (V)					1.3	16.9		104	
LMO5 Cc-B+	Cava Montaretto	44°11′46.44″	009°35′20.46″	O	CC (V)					1.9	16.8		104	
LMO6+	Cava Montaretto	44°11′46.44″	009°35′20.46″	O	O (WR)	7.247	7.142	1050	1.9	2.3	16.3	−26.0	109	
LMO8 Cc-A+	Cava Montaretto	44°11′46.44″	009°35′20.46″	B	CC (V)					2.4	16.8		104	
LMO9-A+	Cava Montaretto	44°11′46.44″	009°35′20.46″	B	B (M)					2.5	16.1		111	
LMO9-B+	Cava Montaretto	44°11′46.44″	009°35′20.46″	B	S (clt)					−1.5	15.6		116	
LMO9-C+	Cava Montaretto	44°11′46.44″	009°35′20.46″	B	S (clt)									
LMO9-D+	Cava Montaretto	44°11′46.44″	009°35′20.46″	B	S (clt)				−6.5					
LMO13+	Cava Montaretto	44°11′46.44″	009°35′20.46″	B	B (WR)				1.2	2.4	16.2	−26.3	110	
LMO13 Cc-A+	Cava Montaretto	44°11′46.44″	009°35′20.46″	B	CC (V)					2.6	17.2		100	
LMO17+	Cava Montaretto	44°11′46.44″	009°35′20.46″	CC	CC					2.0	17.0		103	
LMO18+	Cava Montaretto	44°11'46.44″	009°35′20.46″	CC	CC					2.1	16.0		112	
LMO19+	Cava Montaretto	44°11′46.44″	009°35′20.46″	S	S (WR)	0.166	0.148	180	−3.3	−2.9	17.4	−26.4	99	
LMO20+	Cava Montaretto	44°11′46.44″	009°35′20.46″	S	S (WR)	0.042	0.028	135	−12.6	<l.o.d.	<l.o.d.	−25.6		9.3
LMO20Cc-B+	Cava Montaretto	44°11′46.44″	009°35′20.46″	S	CC (V)					−0.4	18.3		90	
LMO21+	Cava Montaretto	44°11′46.44″	009°35′20.46″	S	S (WR)	0.043	0.030	131	−8.7	<l.o.d.	<l.o.d.	−26.0		
LMO21 Cc-A+	Cava Montaretto	44°11′46.44″	009°35′20.46″	S	CC (V)					−0.9	17.8		95	
LMO21 Cc-B +	Cava Montaretto	44°11′46.44″	009°35′20.46″	S	CC (V)					−0.6	15.9		113	
LMO21 Cc-D+	Cava Montaretto	44°11′46.44″	009°35′20.46″	S	CC (V)					−0.7	15.7		115	
LMO21 Cc-E+	Cava Montaretto	44°11′46.44″	009°35′20.46″	S	CC (V)					−0.7	15.6		116	
LMO22+	Cava Montaretto	44°11′46.44″	009°35′20.46″	Blt	Blt (WR)	0.014	0.003	111	−10.0	<l.o.d.	<l.o.d.	−27.1		
LMO25+	Cava Montaretto	44°11′46.44″	009°35′20.46″	S	S (WR)	0.826	0.786	402	−1.7	−1.4	15.5	−22.8	117	9.3
LMO26a+	Cava Montaretto	44°11′46.44″	009°35′20.46″	S	S (WR)	1.130	1.081	492	−1.8	−1.4	17.1	−24.6	101	
102308 1-1*	Cava dei Marmi	44°11′51.06″	009°35′20.7″	Dark gray		0.028			−9.9			−19.9		
102308 4-1*	Cava dei Marmi	44°11′51.06″	009°35′20.7″	Dark gray block		0.050	*0.038*	118	−4.2			−19.0		

102308-7*	Cava dei Marmi	44°11′51.06″	009°35′20.7″	dk gray		0.039	*0.026*	132	−9.7			−18.4		
102308-8*	Cava dei Marmi	44°11′51.06″	009°35′20.7″	dk gray				119				−19.9		
102308-10*	Cava dei Marmi	44°11′51.06″	009°35′20.7″	Red metasomatized		1.785	*1.778*	73	1.1					
102308-12*	Cava dei Marmi	44°11′51.06″	009°35′20.7″	Dark gray		0.053	*0.042*	111	−8.7			−25.1		
LA1+	Cava dei Marmi	44°11′51.06″	009°35′20.7″	S	S (WR)	0.038	0.020	180	−8.1	<l.o.d.	<l.o.d.	−25.7		9.9
LA2 Oph-A+	Cava dei Marmi	44°11′51.06″	009°35′20.7″	O	O (M)	0.709	0.705	43	−0.2	1.1	16.8		104	
LA2 Oph-B+	Cava dei Marmi	44°11′51.06″	009°35′20.7″	O	O (M)	1.464	1.436	277	0.9	1.5	18.5		89	
LA2 Cc-A+	Cava dei Marmi	44°11′51.06″	009°35′20.7″	O	CC (V)					2.0	24.2		49	
LA2 Cc-B+	Cava dei Marmi	44°11′51.06″	009°35′20.7″	O	CC (V)					1.7	20.0		77	
LA3a+	Cava dei Marmi	44°11′51.06″	009°35′20.7″	S	S (WR)	0.798	0.775	230	−0.5	0.2	16.9	−26.2	103	9.4
LA3b+	Cava dei Marmi	44°11′51.06″	009°35′20.7″	S	S (WR)	2.345	2.342	27	0.1	0.4	16.9	−25.6	103	
LA3 Cc-A+	Cava dei Marmi	44°11′51.06″	009°35′20.7″	S	CC (V)					2.3	19.2		83	
LA3 Cc-B+	Cava dei Marmi	44°11′51.06″	009°35′20.7″	S	CC (V)					2.8	22.4		60	
LA4+	Cava dei Marmi	44°11′51.06″	009°35′20.7″	O	O (WR)	1.722	1.705	170	1.2	1.7	16.4	−26.3	108	
LA4 Oph+	Cava dei Marmi	44°11′51.06″	009°35′20.7″	O	O(M)	0.914	0.895	187	0.3	1.3	16.2	−26.1	110	
LA5 Cc-A+	Cava dei Marmi	44°11′51.06″	009°35′20.7″	O	CC (V)					2.2	19.5		81	
LA5 Cc-B+	Cava dei Marmi	44°11′51.06″	009°35′20.7″	O	CC (V)					2.3	19.4		82	
LA5 Oph+	Cava dei Marmi	44°11′51.06″	009°35′20.7″	O	O (M)	1.941	1.921	203	1.1	1.6	16.2	−26.6	110	
LA6Oph +	Cava dei Marmi	44°11′51.06″	009°35′20.7″	O	O (M)	1.413	1.391	220	1.2	1.5	15.8	−26.7	114	
LA6Serp-A+	Cava dei Marmi	44°11′51.06″	009°35′20.7″	O	S (clst)				−13.0					
LA6Cc-A+	Cava dei Marmi	44°11′51.06″	009°35′20.7″	O	CC (V)					2.4	20.6		73	
LA6Cc-B+	Cava dei Marmi	44°11′51.06″	009°35′20.7″	O	CC (V)					2.2	19.2		83	
LA6Cc-C+	Cava dei Marmi	44°11′51.06″	009°35′20.7″	O	CC (V)					2.7	17.6		97	
LA7Oph+	Cava dei Marmi	44°11′51.06″	009°35′20.7″	O	O (M)	0.414	0.367	467	−0.9	0.1	16.2		110	
LA7Mik+	Cava dei Marmi	44°11′51.06″	009°35′20.7″	O	O (M)		9.668			2.2	17.6		97	
LA7Cc-A+	Cava dei Marmi	44°11′51.06″	009°35′20.7″	O	CC (V)					2.7	22.3		61	
LA7Cc-B+	Cava dei Marmi	44°11′51.06″	009°35′20.7″	O	CC (V)					2.2	18.9		86	
LA8+	Cava dei Marmi	44°11′51.06″	009°35′20.7″	S	S (WR)	0.027	0.017	103	−6.8		<l.o.d.	−23.8		
LA9+	Cava dei Marmi	44°11′51.06″	009°35′20.7″	S	S (WR)	0.451	0.436	150	0.1	−0.2	15.9	−24.2	113	
LA10+	Cava dei Marmi	44°11′51.06″	009°35′20.7″	B	B (WR)	5.878	5.865	128	2.2	1.8	17.7	−26.5	96	
LA12+	Cava dei Marmi	44°11′51.06″	009°35′20.7″	S	S (WR)	0.053	0.025	273	−9.7	<l.o.d.	<l.o.d.	−24.4		
LA14+	Cava dei Marmi	44°11′51.06″	009°35′20.7″	S	S (WR)	0.033	0.016	171	−13.6	<l.o.d.	<l.o.d.	−24.2		
LA15+	Cava dei Marmi	44°11′51.06″	009°35′20.7″	S	S (WR)	0.033	0.019	141	−8.0	<l.o.d.	<l.o.d.	−25.0		
LA16+	Cava dei Marmi	44°11′51.06″	009°35′20.7″	S	S (WR)	0.115	0.102	125	−1.8	<l.o.d.	<l.o.d.	−26.2		
102408 5A*	Cava San Giorgio	44°11′25.6″	009°35′43.8″			0.049	*0.023*	260	−9.4			−18.9		
102408 5B*	Cava San Giorgio	44°11′25.6″	009°35′43.8″			0.146	*0.117*	290	−5.5			−19.2		
102408 5C*	Cava San Giorgio	44°11′25.6″	009°35′43.8″			3.682	*3.658*	240	−0.9			−20.8		
102408 6*	Cava San Giorgio	44°11′25.6″	009°35′43.8″			0.045	*0.020*	250	−9.8			−16.9		
102408 7*	Cava San Giorgio	44°11′25.6″	009°35′43.8″			1.545			−1.8					
102408 8*	Cava San Giorgio	44°11′25.6″	009°35′43.8″			0.084	*0.060*	240	−6.8			−23.0		
102408 9*	Cava San Giorgio	44°11′25.6″	009°35′43.8″			5.719	*5.696*	230	−1.7			−24.4		
LRO1+	Cava San Giorgio	44°11′25.6″	009°35′43.8″	S	S (WR)	0.032	0.012	198	−12.7	<l.o.d.	<l.o.d.	−24.8		
LRO3+	Cava San Giorgio	44°11′25.6″	009°35′43.8″	S	S (WR)	0.029	0.012	170	−12.6	<l.o.d.	<l.o.d.	−24.6		
102408 10-1*	Cava Sfinge	44°13′49.47″	009°36′25.12″			1.132	*1.109*	231	−1.7			−23.5		
102408 10-2*	Cava Sfinge	44°13′49.47″	009°36′25.12″			0.352	*0.340*	120	−2.0			−24.6		
102408 11*	Cava Sfinge	44°13′49.47″	009°36′25.12″			0.995	*0.984*	109	−1.7			−21.2		
102308 16*	Mt Agata Quarry	44°13′47.49″	009°36′21.73″			4.196	*4.185*	112	−1.1			−18.5		
102308 17*	Mt Agata Quarry	44°13′47.49″	009°36′21.73″			2.254	*2.243*	107	−1.2			−20.4		
072706-1*	ValGravalia roadcut serp	44°20′42.24″	009°27′25.55″											
LPA1+	Cava Pavaretto	44°15′52.74″	009°35′13.74″	S	S (WR)	0.022	0.007	148	−16.4	<l.o.d.	<l.o.d.	−25.0		
LPA3-A+	Cava Pavaretto	44°15′52.74″	009°35′13.74″	O/B	S (clst)					0.0	16.2		110	
LPA3Cc-A+	Cava Pavaretto	44°15′52.74″	009°35′13.74″	O/B	CC (V)					2.4	18.5		89	

[a] Sample name: samples measured at Ann Arbor are indicated by*, samples measured in Zurich are indicated by +.
[b] Rock type: description of the whole rock sample; S = serpentinite; O = ophicalcite; B = breccia; Blt = basalt; CC = calcite crystals.
[c] Analyzed part: analyzed part of the rock; WR = whole rock; CC = calcite; V = vein; M = matrix; clst = clast.
[d] In italic: TIC values calculated from TIC = TC−TOC.
[e] Temperature calculated using the equation: $1000\ln\alpha = 2.78(10^6 * T^{-2}) - 2.89$ from Friedman and O'Neil (1977).

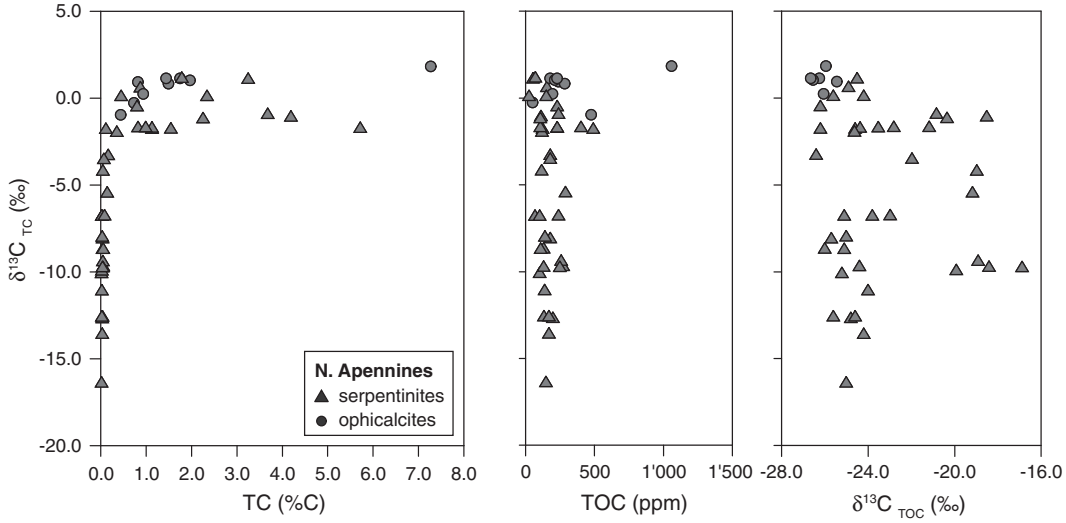

Fig. 5. Total carbon (TC) and total organic carbon (TOC) contents and isotope composition of serpentinites and ophicalcites from the Northern Apennines. High total carbon contents are dominated by inorganic carbon, which is characterized by $\delta^{13}C$ values of approximately 0‰, also indicating incorporation of seawater carbonate. $\delta^{13}C$ of the organic carbon (TOC) has a range between −27.1 and −16.9‰ (Table 3).

average of $\delta^{18}O = 9.5 \pm 0.3$‰, while one sample of serpentinite at Cava Galli preserves a lower value of 6.7‰ and thus indicates higher alteration temperatures. These values lie within the range of serpentinite samples analyzed by Barrett and Friedrichsen (1989) and are enriched in ^{18}O compared to pristine mantle peridotite (5.8 ± 0.3‰; Taylor, 1968; Kyser, 1986; Mattey et al., 1994). Barrett and Friedrichsen (1989) also analyzed two serpentine–magnetite pairs with similar values, yielding $\Delta_{serpentine-magnetite} = 8.2$ and 11.9‰, respectively, and calculated serpentinization temperatures of 240 and 130 °C, respectively.

5. Discussion

5.1. Fluid circulation inferred from carbon geochemical signatures

A major component of carbon in oceanic serpentinites is inorganic carbon that is incorporated during seawater circulation and is reflected by $\delta^{13}C_{TIC}$ of 0 ± 2‰ at the Iberian Margin and by values of 0 ± 3‰ in the N. Apennine serpentinites and ophicalcites. In marine hydrothermal systems, calcium in calcite or aragonite is generally derived from the fluid, whereas dissolved inorganic carbon (DIC) is mainly derived from seawater (Früh-Green et al., 2003; Palandri and Reed, 2004; Ludwig et al., 2006). Hydrothermal fluids may contribute small amounts of CO_2 resulting in the observed small deviations from a $\delta^{13}C_{TIC}$ of 0‰. These isotopic variations can be caused by oxidation of ^{13}C-depleted methane (or another reduced carbon species), which is commonly formed during serpentinization (e.g. Berndt et al., 1996) and would produce ^{13}C-depleted CO_2, or by reduction of CO_2 to methane, which leads to a ^{13}C-enrichment of the residual CO_2 (Früh-Green et al., 2003).

At the Iberian Margin, the highest inorganic carbon contents are observed at 660–675 mbsf at Site 897C and at 740–760 mbsf at Site

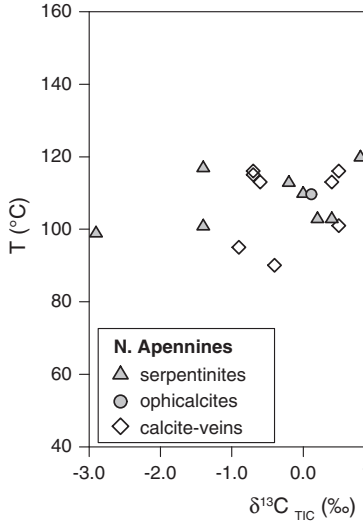

Fig. 6. Calculated calcite precipitation temperatures from oxygen isotopes from calcite veins (diamonds) extracted from various serpentinite and ophicalcite samples (N. Apennines). Circles are bulk rock or matrix values from ophicalcites; triangles are bulk rock values from serpentinites. Temperatures reveal a range in temperature from ~50 to 150 °C.

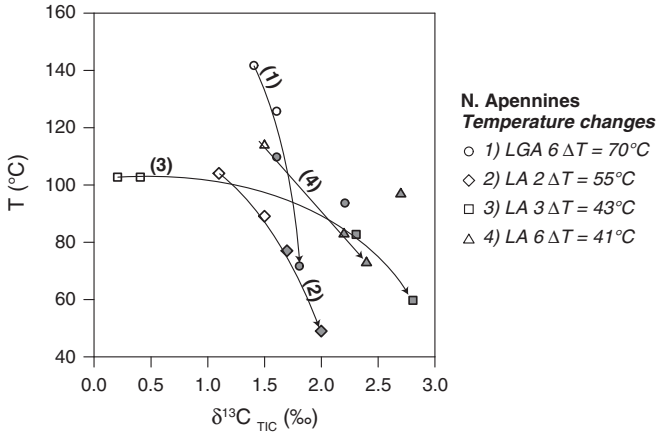

Fig. 7. Calcite formation temperatures of different vein-generations from four ophicalcite rock samples collected at Cava Galli (LGA 6) and Cava dei Marmi (LA2, LA3, LA6) in the Northern Apennines. Empty symbols: very fine-veined ophicalcite matrix, representing the earliest stages of vein formation; full symbols: calcite veins, which cut the matrix. Detailed petrographic study of the relation between the extracted calcite veins clearly reveals a decrease in precipitation temperature from old to young vein-generations. Sample LGA6 (no. 1; from Cava Galli) gives the largest temperature difference of 70 °C between the fine-veined ophicalcite matrix and late calcite veins. In the Cava dei Marmi, sample LA2 (no. 2) yields the largest temperature difference of 55 °C between the fine-veined matrix and late calcite veins, while sample LA3 (no. 3) shows a temperature difference of 43 °C and sample LA6 (no. 4) a difference of 41 °C.

897D (Fig. 4) just above zones of cold shearing within the serpentinites. This suggests that circulation of fluids and seawater through the oceanic crust is predominantly controlled by shear- and fault zones, which facilitate introduction of large amounts of fluids into the system. This is also supported by the sulfur geochemistry. In samples recovered during Leg 173, Schwarzenbach et al. (2012) found a loss of sulfides through oxidation and high fluid flux along shear zones, which are accompanied by an increase in sulfate with a seawater composition. In contrast, at depth and below major fault zones, extensive time-integrated fluid circulation (with high fluid through-flow) is limited, as indicated by the significantly lower inorganic carbon contents at greater depth at the Iberian Margin. These observations are in agreement with studies of Alt and Teagle (1999) who showed that the carbonate content of altered oceanic crust decreases with depth. They showed that fluid circulation in the porous upper volcanic section can continue for as long as 100 Ma and that the highest abundance of carbonate veins is correlated with zones of high porosity and permeability. During serpentinization, conversion of olivine and pyroxene to serpentine is accompanied by a volume increase of up to 40% (O'Hanley, 1996), which creates microfractures and propagates cracks (Martin and Fyfe, 1970; Macdonald and Fyfe, 1985; Andreani et al., 2007). At the same time, precipitation of calcite occurs in open fractures and can also create permeability through in-situ brecciation of the surrounding rocks (Jamtveit et al., 2009, 2011). Thus, these systems are characterized by complex controls on permeability structures and fluid pathways. In addition, Schroeder et al. (2002) suggested that fluid circulation is promoted by tectonic activity, leading to opening of cracks and fractures forming new fluid pathways and therefore also influencing the permeability.

Similarly, in the N. Apennines we observed a significant increase in calcite veins from the bottom of the exposed serpentinite in the quarries to the top of the sections. The pervasive veining in the ophicalcites of this sequence reflects intense fluid circulation within the uppermost part of the uplifted mantle that was exposed to seawater, which is also evidenced by the strongly oxidized state shown by the red color of the ophicalcites (Fig. 3) and the change in temperature discussed below. Treves and Harper (1994) identified various ductile to brittle events in the N. Apennine ophicalcites, which can be linked to tectonic activity in a mid-ocean ridge environment. When major fault zones and cracks are absent, fluid circulation possibly takes place by diffuse porous flow as described by Beard and Hopkinson (2000) for the breccias and serpentinites at Hole 1068 (ODP Leg 173).

Lower time-integrated water–rock ratios and therefore less oxidizing conditions at greater depth in this section are indicated by the color change from red ophicalcites to green serpentinites (Fig. 3), and also by variations in the sulfide and oxide mineralogy. Hematite dominates the ophicalcites, whereas the underlying strongly calcite-veined serpentinites are characterized by the occurrence of pyrite, and the less calcite-veined serpentinites are dominated by more reduced assemblages with magnetite, pyrrhotite, pentlandite, millerite and siegenite (Schwarzenbach et al., 2012).

A similar pattern was observed in the Iberian Margin drillcores by Alt and Shanks (1998) who found an upper carbonate-serpentine zone characterized by pyrite and rare magnetite, and a lower zone characterized by higher amounts of magnetite and sulfur-richer assemblages such as valleriite and rare pentlandite. At Hole 897C this transition coincides approximately with the strong decrease in TIC contents (Fig. 4A). However, at Hole 897D Alt and Shanks (1998) located this transition further down hole than we would infer from inorganic carbon contents (Fig. 4B). This discrepancy could be due to the sulfide mineralogy of the upper sections of Hole 897C as a criterion for defining the carbonate-serpentine zone in the study of Alt and Shanks (1998).

Summarizing, at both locations intense carbonate-veining implies high water–rock ratios in the upper sections of the exposed mantle, which leads to oxidizing conditions, whereas low carbonate contents in the lower sections of the exposed mantle reflect decreasing time-integrated water–rock ratios with depth.

5.2. Temperatures of calcite precipitation in various tectonic settings

Field observations and cathodoluminescence analysis by Treves et al. (1995) on the ophicalcites from the N. Apennines document several generations of calcite-veining and show that the veins have been reactivated numerous times, as indicated by the brecciation of older veins. Our oxygen isotope analyses of the different calcite generations revealed a relatively large temperature range (Fig. 6) and support these observations. In general, the matrix calcite in the ophicalcites, which forms a microscopically fine network of veins penetrating the matrix, was formed at higher temperatures than the wider calcite veins. In addition, cross-cutting relationships among the veins reveal a clear trend of decreasing temperatures from early vein generations to younger, much wider veins. Fig. 7 shows a selection of four ophicalcite samples showing differences of up to 70 °C between vein generations (see figure description for details). In contrast, the bulk rock serpentinites characterized by low TIC contents show a narrow temperature range (99–120 °C; Fig. 6 and Table 3). These results demonstrate a decrease in temperature with increasing fracturing of the serpentinites and document that temperature conditions varied with each vein-generation.

The calculated calcite precipitation temperatures at the Iberian Margin are lower than those found in the N. Apennine ophiolites. The temperatures we calculated (19–44 °C) agree with those of Agrinier et al. (1996) and are slightly higher than ambient seawater. We observe no clear trend with depth but isolated carbonate veins tend to show slightly higher temperatures (<44 °C) than the bulk rock. At the Iberian Margin, mantle rocks were exposed to seawater during the final stage of continental rifting, just before seafloor spreading started (Sawyer et al., 1994). Presumably, the carbonate formation temperatures reflect the small temperature gradients within the lithosphere at this stage of rifting. This could be due to the absence of volcanism (Whitmarsh and Wallace, 2001) or because the exposed ultramafic body had already cooled with no other heat source than residual mantle heat.

Significant differences in carbonate precipitation temperatures are found in various peridotite-hosted hydrothermal systems (Table 4). Calcite veins in serpentinites from the MARK area (Mid-Atlantic Ridge Kane fracture zone) show formation temperatures between 1 and 235 °C (Alt and Shanks, 2003), while carbonate veins near the 15°20′N Fracture Zone (ODP Leg 209) show temperatures of less than 14 °C for aragonite in serpentinites and up to 170 °C for calcite in detachment fault rocks (Bach et al., 2011). Both the MARK area and the 15°20′N Fracture Zone are located along the Mid-Atlantic Ridge, where young mantle has been exposed by detachment faulting (Karson and Lawrence, 1997; Alt and Shanks, 2003; Schroeder et al., 2007; Bach et al., 2011). The carbon isotope compositions of the veins suggest that they are of seawater origin. At Sites 1271 and 1274 from Leg 209, formation temperatures of aragonite increase from ambient seawater to 14 °C with increasing depth, suggesting precipitation during extensive seawater penetration in the last stages of mantle exhumation (Bach et al., 2011). Locally they preserve a higher temperature gradient (100–150 °C/km) over a depth of 85 m, which is attributed to the rapid uplift of the ultramafic rocks and continued cooling, while temperatures of up to 170 °C of the calcites are attributed to cooling of higher-temperature hydrothermal fluids circulating along the detachment fault (Bach et al., 2011). Carbonates analyzed from the LCHF reveal a similarly wide range of precipitation temperatures of 2 to 225 °C (Früh-Green et al., 2003; Früh-Green unpublished data), where mixing of alkaline fluids with seawater produces fracture-filling precipitates in the serpentinite basement and chimney-like structures atop the basement. However, samples from the basement of the LCHF were sampled by submersible

Table 4
Serpentinization and carbonate precipitation temperatures of peridotite-hosted hydrothermal systems.

	δ^{18}O bulk rock	Δ^{18}Oserp-mgt	Serpentinization temperatures	Reference	Carbonate precipitation	Reference
Ligurian ophiolite	6.7–9.9‰		<240 °C	This study	49–151 °C	This study
Ligurian ophiolite	7.0–10.8‰	8.2‰; 11.9‰	<240 °C	Barrett and Friedrichsen (1989)		
Iberian Margin (ODP Site 897)	5.3–9.3‰ [b]; 8.6–14.2‰ [c]	10.1‰	<100–150 °C	This study	19–44 °C	This study
Iberian Margin (ODP Site 897)	8.8–12.2‰ [b]	11.0‰; 12.5‰	<150 °C	Agrinier et al. (1996)	13–19 °C	Agrinier et al. (1996)
Atlantis Massif	1.7–6.4‰		150–250 °C	Boschi et al. (2008)	2–225 °C	Früh-Green et al. (2003), Früh-Green unpublished data
MAR 15°20′N (Sites 1268, 1271)	2.6–4.4‰		~250–350 °C	Alt et al. (2007)	<14 °C; 80–170 °C [a]	Bach et al. (2011)
MAR 15°20′N (Sites 1272, 1274)	<8.1‰		<150 °C	Alt et al. (2007)	<14 °C	Bach et al. (2011)
MAR 23°N (ODP Sites 920, 670)		3.8–5.1‰	>350 °C	Agrinier and Cannat (1997)	1–235 °C	Alt and Shanks (2003)
Hess Deep (ODP Site 895)	2.2–4.0‰		400 ± 50 °C	Früh-Green et al. (1996)		

[a] Calcite in detachment fault rocks.
[b] δ^{18}O value from serpentine separates.
[c] δ^{18}O value from separated serpentine veins.

and dredging and hence only comprise the more accessible surface of the exposed peridotite.

5.3. Serpentinization temperatures

Serpentinization has been documented to take place over a large temperature range from up to 400–500 °C to as low as 150 °C (e.g. Cannat et al., 1992; Früh-Green et al., 1996; Agrinier and Cannat, 1997; Mével, 2003; Früh-Green et al., 2004; Alt et al., 2007; Boschi et al., 2008). Table 4 shows a compilation of published serpentinization temperatures.

The Iberian Margin is a typical example for low-temperature alteration. The δ^{18}O values of the serpentine–magnetite thermometry indicate serpentinization temperatures of around 150 °C, in agreement with Agrinier et al. (1996). Similarly low temperatures are found at the MAR 15°20′N Fracture Zone (ODP Leg 209), where $\delta^{18}O_{WR}$ values of up to 8.1‰ at Sites 1272 and 1274 suggest temperatures below 150 °C (Alt et al., 2007). Higher δ^{18}O values of up to 14.2‰ have only been found in the separated serpentine veins from the Iberian Margin, suggesting that locally, during late stages of serpentinization, temperatures were probably less than 100 °C. At the Iberian Margin, late alteration of the serpentinites is documented by the presence of palygorskite and vermiculite (Plas, 1997). The serpentine samples containing clay minerals (149-5, 149-50 and 149-53), yield clearly higher δ^{18}O-values (11.3–13.2‰) than the pure serpentine ones (Table 1). By simple mass balance calculations it can be estimated that if 30% of the separated fraction consists of clay minerals, the $\delta^{18}O_{clay}$ would be ~24‰, and if the clay proportion would be 40% the $\delta^{18}O_{clay}$ would be ~20‰. Although oxygen fractionation factors of vermiculite have not been determined experimentally, temperatures well below 100 °C are obtained if a fractionation factor similar to other clays is used (Muehlenbachs and Clayton, 1976; Savin and Lee, 1988). This suggests that clay alteration of Leg 149 serpentinites occurred after serpentinization but predominantly before calcite formation.

The N. Apennine serpentinites are characterized by slightly lower δ^{18}O bulk rock values than the serpentines at the Iberian Margin. Unaltered oceanic peridotites should have bulk rock oxygen isotope ratios within the range known for fresh mid-ocean ridge basalts (5.8 ± 0.3‰; e.g. Taylor, 1968; Kyser, 1986). Seawater–rock interactions produce shifts away from these reference values, whereby the final composition of the rock will reflect the temperatures of alteration and fluid-rock ratios (e.g. Ito and Clayton, 1983; Taylor, 1984). Serpentinites enriched in ^{18}O compared to fresh mantle generally indicate alteration temperatures of less than 200 °C if seawater is the interacting fluid (Wenner and Taylor, 1973; Sakai et al., 1990; Früh-Green et al., 1996; Alt et al., 2007). Assuming high water–rock ratios (>1), we estimate serpentinization temperatures up to 180–200 °C for the sample with the lowest δ^{18}O value (after calculations from Alt et al., 2007), while the higher δ^{18}O values of ~9.5‰ correspond to temperatures of alteration <150 °C. If we assume lower water–rock ratios of <1, temperatures could have been as low as 100 °C. These temperatures are consistent with stability fields of the mineral assemblages observed in these rocks (Schwarzenbach, 2011) and with oxygen isotope temperatures from two serpentine–magnetite pairs (240 and 130 °C, respectively), calculated by Barrett and Friedrichsen (1989).

Mineralogical observations also indicate that serpentine veining was at least locally concurrent with calcite veining (Schwarzenbach, 2011), which occurred at <50–150 °C. Thus, we infer that serpentinization temperatures decreased from ~240 °C to <150 °C, where late serpentine veins reopened calcite veins. Our data also suggest that a distinct low temperature signature overprinted the serpentinites from Cava dei Marmi and Cava Montaretto (Table 3). Similar temperatures as in the N. Apennines are reported for the basement of the LCHF (200 ± 50 °C; Boschi et al., 2008). In contrast, serpentinization temperatures of >250–350 °C at the MARK area and the 15°20′N Fracture Zone (ODP Sites 1268 and 1271) are considered to reflect the influence of a nearby heat source (Alt and Shanks, 2003; Alt et al., 2007). Even higher temperatures are recorded in the Hess Deep serpentinites, where complex tectonic processes likely led to the penetration of seawater-dominated fluids during early stages of the propagation of the Cocos-Nazca rift, inducing serpentinization at temperatures >450 °C (Früh-Green et al., 1996).

In summary, serpentinization and carbonate precipitation at the Iberian Margin took place at lower temperatures than in the N. Apennine serpentinites or most modern ridge-related serpentinites. We infer that at the Iberian Margin, serpentinization occurred at temperatures around 150 °C and decreased with serpentine vein formation to temperatures as low as 100 °C. Late alteration and formation of clay minerals occurred at temperatures less than 100 °C, likely as low as 50 °C, while late calcite precipitation occurred at 19–44 °C. In the N. Apennines, serpentinization temperatures are inferred from serpentine–magnetite pairs and bulk rock serpentinites yielding <150–240 °C. Importantly, temperatures derived from bulk rock serpentine separates or from serpentine–magnetite pairs represent time-integrated signals for the long-lived processes of emplacement, alteration and cooling of mantle peridotites. Serpentine from bulk rocks always represent a mixture of temperatures that occur as a sequence of reactions. This is for example reflected in the temperature range observed in bulk rock and serpentine vein analyses from the Iberian Margin. The temperature range observed in the N. Apennine

serpentinites and ophicalcites overlaps with those observed in the basement of the LCHF (Früh-Green et al., 2003; Boschi et al., 2008), but is lower than in peridotite-hosted hydrothermal systems that have a strong influence from a gabbroic heat source, such as the Rainbow hydrothermal field and the MARK area (e.g. Fouquet et al., 1997; Alt and Shanks, 2003). At the Atlantis Massif, fluids likely circulate through faults and interact with the cooling lithosphere (Allen and Seyfried, 2004), before they vent at temperatures less than 100 °C in the carbonate towers (Kelley et al., 2001). Faults and fractures in the N. Apennine serpentinites could similarly have permitted initiation of serpentinization at fairly high temperatures and continued during the cooling of the exposed mantle. Hence, we conclude that the temperature of the serpentinizing body has no major influence on the extent of carbonate formation, but that the presence of faults and therefore tectonic activity primarily controls carbonate storage. In the Ligurian paleo-stockwork serpentinites, the tectonic history is characterized by several phases of deformation (Treves and Harper, 1994) that opened fluid pathways and enabled carbonate formation at continuously decreasing temperatures.

5.4. Sources and cycling of organic carbon

In addition to inorganic carbon derived from seawater, the total carbon contents measured in the serpentinites include a component of organic carbon. Organic carbon in hydrothermal systems can have different origins: 1) incorporation of dissolved or particulate organic carbon from seawater circulation through the oceanic lithosphere; 2) biogenic carbon, produced in-situ through microbial activity in the basement rocks; 3) a thermogenic origin through thermal decomposition of organic matter within the basement rocks or from overlying sediments; 4) an abiogenic origin through Fischer–Tropsch-Type (FTT) reactions; and 5) mantle carbon originating magmatically or from organic matter in sediments that were subducted and recycled back into the mantle (Delacour et al., 2008).

Fig. 8 compares the carbon contents and isotope signatures of the serpentinites from the Iberian Margin, the N. Apennines and the basement of the LCHF at the Atlantis Massif. The correlation between the $\delta^{13}C_{TC}$ and TC contents reflects the dominance of inorganic carbon at high TC contents and the dominance of organic carbon at low TC contents. The carbon isotope compositions of TOC of the analyzed samples from the Iberian Margin are generally more depleted (average $\delta^{13}C_{TOC} = -26.8‰$) than those in the serpentinites and ophicalcites from the N. Apennines (average $\delta^{13}C_{TOC} = -23.8‰$) and the serpentinites from the Atlantis Massif (average $\delta^{13}C_{TOC} = -25.5‰$). Marine dissolved organic carbon (DOC) typically has $\delta^{13}C$ values between approximately −23.5 and −19.5‰ (Druffel et al., 1992; Bauer, 2002 and references therein). Delacour et al. (2008) argue that during extensive water–rock interaction at the Atlantis Massif, DOC may be incorporated into the oceanic crust, contributing to $\delta^{13}C_{TOC}$ values between −28.9 and −21.5‰ in the basement rocks. The overall range of $\delta^{13}C_{TOC}$ values observed at all of the three locations, however, cannot solely reflect input of marine DOC, but rather organic carbon derived from a mixture between DOC and a source that is more depleted in ^{13}C.

TOC contents are comparatively high at the Iberian Margin (Fig. 8). High TOC contents are specifically found at >770 mbsf at Hole 897D, where the TOC accounts for on average ~70% of the total carbon (Fig. 4). Alt and Shanks (1998) and Schwarzenbach et al. (2012) have studied the sulfur geochemistry of the serpentinites from the Iberian Margin ODP Leg 149 and 173, respectively. These serpentinites generally preserve ^{34}S-depleted sulfides formed by microbial sulfate reduction, while the opaque mineral assemblages, especially from Hole 897D, suggest fairly high f_{H2} in the lower sections of the drill cores and point to enhanced availability of H_2 as an energy source for microbes compared to the upper sections. Fig. 9 illustrates the relation of the carbon and the sulfur signatures with sulfur data from Schwarzenbach et al. (2012) and Alt and Shanks (1998; Leg 149). Strongly negative $\delta^{13}C_{TC}$ values generally correlate with strongly negative $\delta^{34}S_{sulfide}$, which reflects extensive microbial activity (i.e. microbial sulfate reduction to form ^{34}S depleted sulfide) and a distinct dominance of organic carbon over inorganic carbon (i.e. high TOC contents) specifically in the samples from the Iberian Margin (dark gray areas in Fig. 9). These samples are also characterized by high sulfide contents that likely result from microbial sulfate reduction to form sulfide. At high water–rock ratios, biomass production is obscured by the input of higher amounts of carbonate from seawater (dotted line in Fig. 9). Precipitation of seawater carbonate leads to a shift of the $\delta^{13}C_{TC}$ values of the serpentinites towards 0‰. Thus, the trend indicated by the black arrow in Fig. 9 indicates a decrease in input of seawater DIC and an increasing contribution of organic carbon associated with microbial reduction of seawater sulfate (Jurassic and Cretaceous $\delta^{34}S_{seawater-sulfate} = 14–17‰$;

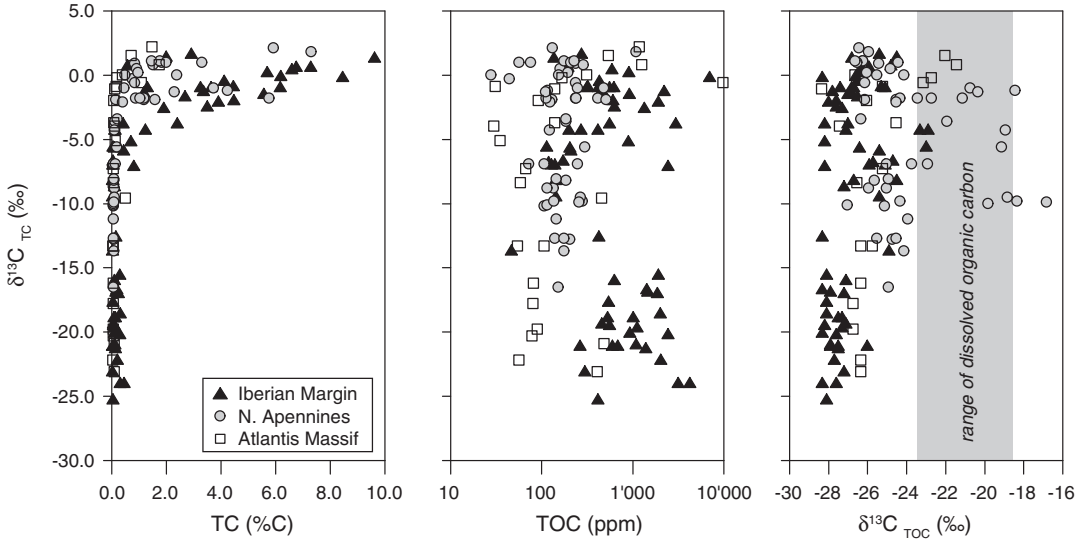

Fig. 8. Comparison of total carbon (TC) and total organic carbon (TOC) contents and isotope compositions of serpentinites from the Iberian Margin, from the Northern Apennines, and from the Atlantis Massif (data from Delacour et al., 2008). TOC contents are plotted on a logarithmic scale. TC data reflects the mixing between isotopically light organic carbon and inorganic carbon with an isotopic composition around 0‰ typically found in marine carbonates. Marine dissolved organic carbon has an average composition of −23.5 to −19.5‰ (Druffel et al., 1992; Bauer, 2002 and references therein).

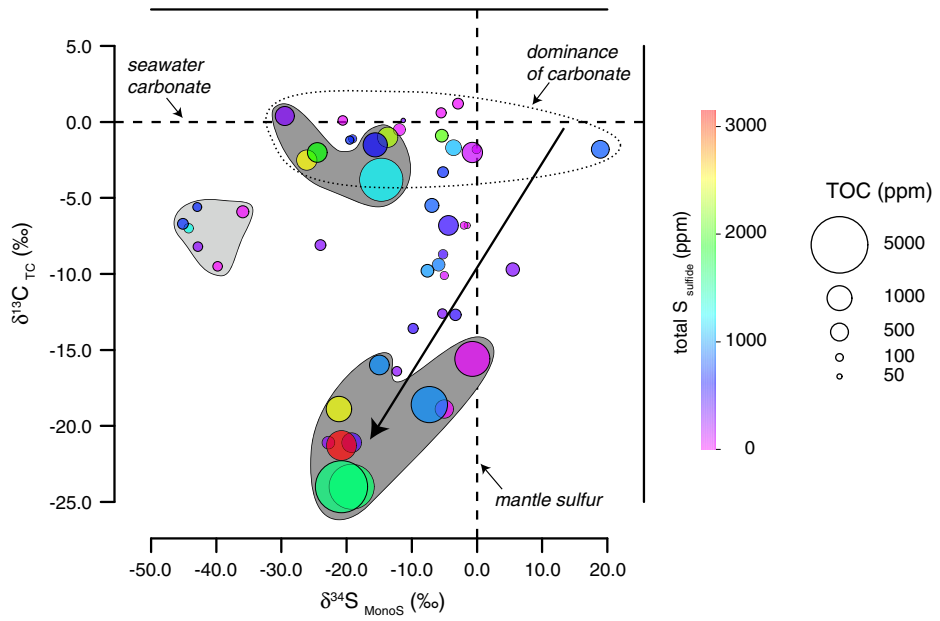

Fig. 9. Comparison between the carbon and sulfur signatures of serpentinites from the Iberian Margin Leg 149 (dark gray areas), Leg 173 (light gray area) and the N. Apennines (circles not in a shaded field). Sulfur data are from Schwarzenbach et al. (2012) and Alt and Shanks (1998; Leg 149). The x- and y-axis show $\delta^{34}S_{sulfide}$ against $\delta^{13}C$ of total carbon (TC), respectively. Bubble sizes show variations in TOC content (logarithmic scale with content proportional to bubble size). The bubble color shows variations in total sulfide content of the bulk rock samples. The black arrow indicates a change in input of seawater DIC and a trend from carbonate-dominated serpentinites (and domination of seawater sulfate with $\delta^{34}S = 14–17‰$ for Jurassic seawater; Kampschulte and Strauss, 2004) to serpentinites that are dominated by organic carbon associated with microbially produced ^{34}S-depleted sulfide. High microbial activity with formation of negative $\delta^{34}S_{sulfide}$ values results in comparatively higher amounts of TOC and commonly higher sulfide contents in samples from Leg 149 (dark gray areas). A dominance of $\delta^{34}S_{sulfide}$ values of −10 to 0‰ mainly in the serpentinites from the N. Apennines can be attributed to other processes that affect the sulfide isotope composition in serpentinites (e.g. hydrothermal sulfide addition, sulfide oxidation; Schwarzenbach et al., 2012). The dotted line indicates the dominant influence of inorganic carbon resulting in $\delta^{13}C_{TC}$ values around 0‰.

Kampschulte and Strauss, 2004) to ^{34}S depleted sulfide with progression to lower water–rock ratios. Sulfate-reducing microbes not only use SO_4 as electron acceptor while oxidizing organic compounds (e.g. Trudinger et al., 1985), but can also fix CO_2 by the reductive acetyl CoA pathway producing strongly ^{13}C depleted organic carbon (Londry and Des Marais, 2003; Lever et al., 2013). Additionally, sulfate-reducing microbes may live in symbiosis with methanogenic archaea that reduce CO_2 to CH_4 (e.g. Alperin and Hoehler, 2009). Thus, a consortium of microbes supported by the availability of H_2 produced during serpentinization and availability of low amounts of CO_2 could have allowed conversion of CO_2 to organic carbon concurrent with microbial conversion of seawater sulfate to H_2S, resulting in both an increase of sulfide and organic carbon. Since microbial activity is limited to low temperatures (<122 °C; Elsgaard et al., 1994; Stetter, 1996; Takai et al., 2008) the low alteration temperatures at the Iberian Margin allowed for and likely enhanced biological activity.

Summarizing, low serpentinization temperatures and availability of H_2 at low water–rock ratios both facilitated extensive microbial sulfate reduction at the Iberian Margin, as was also suggested by Alt and Shanks (1998). This likely caused the production of higher amounts of biomass in the rocks from the Iberian Margin compared to the N. Apennines and the Atlantis Massif (Fig. 8) and also resulted in a dominance of organic carbon over inorganic carbon (mainly due to less input of inorganic carbon) in the lower sections of the exposed mantle (Fig. 4).

5.5. Carbon sequestration in serpentinites

Various studies have recently demonstrated that carbonate precipitation in serpentinizing environments is a strongly reactive process and that serpentinization needs to be considered as a major sink in the global carbon cycle (Cipolli et al., 2004; Früh-Green et al., 2004; Andreani et al., 2008; Kelemen and Matter, 2008; Matter and Kelemen, 2009). The results of our study document that during serpentinization significant amounts of carbonate (with up to 9.6 wt.% TIC in the ophicalcites) are fixed within the oceanic lithosphere. To evaluate the extent and importance of carbon storage during serpentinization, we propose an estimate of the amount of carbon fixed during serpentinization of exposed mantle rocks on the ocean floor.

We have shown in this study that the extent of carbonate uptake from seawater strongly depends on the presence of faults and fractures. Seismic data of the Iberian Margin indicate that faults extend as deep as 15 km into the upper lithosphere (Whitmarsh and Wallace, 2001). However, serpentinization and extensive water–rock interaction are likely concentrated around these fault zones and probably decreases strongly with progression away from the faults due to permeability restrictions (Alt and Shanks, 1998; Andreani et al., 2007). Thus, the vertical extension of carbon uptake in the oceanic lithosphere is likely very heterogeneous and therefore difficult to determine. The results from the Iberian Margin revealed an overall decrease in carbon uptake with depth. The observations from the Iberian Margin and the outcrops in the N. Apennines suggest that the uppermost 20–50 m and in some places up to 70 m of the exposed mantle rocks experience intense water circulation leading to the fixation of 3.6–4.7 wt.% of carbon mainly as carbonate. Additionally, the results from the Iberian Margin give evidence that to a depth of ~150 m into the peridotite basement (= thickness of drilled serpentinite section at Hole 897D) extensive microbial activity results in the formation of higher amounts of organic matter and the incorporation of 0.1–0.2 wt.% C. Andreani et al. (2007) proposed that the upper most 7 km of the oceanic lithosphere experiences hydration. Hence, from the low-carbonate serpentinites we estimate that at these depths 0.02–0.05 wt.% C may be fixed as carbonate or organic carbon within the rock.

An important unknown is the amount of mantle rock that is exposed on the ocean floor. A number of recent studies suggest that up to 20% of the ocean floor formed along slow-spreading ridges consists of uplifted serpentinized peridotite (Dick et al., 2008; Smith et al., 2008; Cannat et al., 2010). Using the above assumptions concerning decreasing carbon uptake with depth, an average spreading rate of 22 mm/year at slow-spreading ridges (Cannat et al., 2010), and that 50% of the mid-ocean ridges are slow-spreading ridges (~33,600 km; Carbotte

and Scheirer, 2004) with a mantle exposure of 20%, we calculate that a minimum of 1.1 to 2.7 × 10^{12} g C is fixed annually during serpentinization of exposed mantle rocks on the ocean floor. 30–40% thereof are stored within the uppermost 20–50 m of the exposed mantle (40–45% in the uppermost 150 m) and is dominated by carbonate, while the lower approximately 7 km store 55–60% of the carbon, which is variably dominated by inorganic or organic carbon. The uppermost 50–100 m of serpentinized oceanic lithosphere generally has a dominance of TIC of 80–99%, while at greater depth TOC constitutes 30–96% of the total carbon, strongly depending on addition of seawater carbonate through deep faults. The distribution of inorganic and organic carbon suggests that incorporation of carbon through microbial activity becomes important at depths of >50 m, where temperature conditions and hydrogen availability can sustain microorganisms.

Alt and Teagle (1999) calculated that 4 × 10^{13} g C/year is stored by alteration of Mesozoic oceanic crust, which is one order of magnitude higher than what our estimates for Jurassic peridotite suggest. Importantly, our calculation only comprises the slow-spreading ridges, where mantle rocks are serpentinized by seawater exposure, but do not include carbon uptake during alteration of mafic oceanic crust. Thus, the comparison with Alt and Teagle (1999) suggests that serpentinization of exposed mantle rocks accounts for ~10% of the carbon stored within the oceanic lithosphere. Since peridotites make up 10–20% of the oceanic crust, this implies that carbon uptake per unit volume of peridotite is similar to that of mafic ocean crust (Alt and Teagle, 1999; Shilobreeva et al., 2011).

The global carbon cycle is influenced by complex interactions of the hydrosphere, lithosphere and biosphere, which each comprise of numerous reservoirs. Carbon in the oceans is mainly derived from rivers (8 × 10^{14} g C/year; Siegenthaler and Sarmiento, 1993) and through degassing at mid-ocean ridges (8.4 × 10^{12} g C/year; Gerlach, 1989), while alteration of the oceanic crust and sedimentation (2 × 10^{14} g C/year; Siegenthaler and Sarmiento, 1993) remove carbon from seawater. These fluxes suggest that carbon cycled through alteration of oceanic lithosphere accounts for about 10% of the total carbon that is removed, while carbon stored within serpentinites accounts for about 1%. Respiration of plant material on land has much higher fluxes (10^{17} g C/year; Siegenthaler and Sarmiento, 1993), however, their residence time is generally on the order of decades (Falkowski et al., 2000). Our study has shown that during the Jurassic, carbon was incorporated into the oceanic lithosphere and stored as inorganic carbon and organic carbon within the N. Apennine serpentinites. Thus, during several millions of years carbon was removed from the hydrosphere before it is re-exposed to weathering. Hence, alteration of oceanic crust and its storage over 100 millions of years clearly plays an important role in the long-term cycling of carbon between hydrosphere, lithosphere and biosphere.

6. Summary and conclusions

This study provides new data on the character of fluid circulation and on temperature conditions in peridotite-hosted hydrothermal systems, as well as the importance of carbon sequestration during serpentinization and its long-term preservation. Both of the hydrothermal systems reported here are ancient analogs of modern peridotite-hosted hydrothermal systems and have taken up and fixed marine DIC as calcium carbonate for millions of years. We propose that tectonic activity and the formation of fractures and deep fluid pathways are likely the main factors controlling the amount of carbonate stored, and that the temperature of the serpentinizing peridotite is not very important in terms of carbonate incorporation. In contrast, serpentinization temperatures likely control the presence of microbial activity, which is limited to fairly low temperatures (<122 °C). At the Iberian Margin, low alteration temperatures allowed extensive microbial activity of sulfate-reducing bacteria resulting in enhanced production of biomass (i.e. biotically produced organic carbon) compared to the Atlantis Massif and the N. Apennine serpentinites. Thus, serpentinization temperatures influence the amount of organic carbon stored within serpentinites.

We attribute the generally low temperatures at the Iberian Margin to a relatively low geothermal gradient and low heat flow within the lithosphere as a consequence of continental rifting. Mantle exposure during the last stages of continental rifting preceding the opening of the North Atlantic resulted in serpentinization and formation of carbonates at temperatures lower than observed in the Ligurian ophiolite. The serpentinites from the N. Apennines preserve a cooling history that is very similar to that of the basement of the Atlantis Massif with serpentinization initiating at likely >240 °C. Fracturing and faulting along a mid-ocean ridge probably allowed fluid penetration at high temperatures and during continuous cooling of the exposed mantle to temperatures <50 °C. Thus, our results strengthen the argument that the calcite-vein-network represents the paleo-stockwork of a hydrothermal system analogs to the basement of the LCHF, where exposure of mantle rocks by long lived detachment faulting led to serpentinization over the last million year at high temperatures (200 ± 50 °C) while today fluids vent at low temperatures (<40–90 °C).

We give evidence that serpentinization of ultramafic rocks on the ocean floor accounts for approximately 10% of the carbon cycled through alteration of oceanic lithosphere, with the uppermost 20–50 m of the exposed peridotite incorporating 30–40% of the carbon comprising 80–99% of carbonate, while organic carbon is dominant at depths of >50–100 m. Overall, alteration of oceanic crust recycles approximately 10% of all the carbon that is cycled through the oceans. Even though the oceans represent a small carbon reservoir compared to the biosphere, the study of serpentinites from the Jurassic and Cretaceous provides evidence that peridotite-hosted hydrothermal systems enable carbon storage over several tens of millions of years with much longer residence times compared to the biosphere, suggesting that alteration of oceanic lithosphere plays an important role in the long-term, global carbon cycle.

Acknowledgments

We would like to thank Maria Coray-Strasser, Stewart Bishop, Eric Reusser for help with analyses and Chiara Boschi and Andrea Dini from the University of Pisa for help with the sample collection. We also would like to thank two anonymous reviewers for their helpful comments that improved the manuscript. This research used samples and data provided by the Ocean Drilling Program (ODP). Funding for this research was provided by the Swiss NSF Grant No. 200020-116226 and No. 200020-124669 to Früh-Green. J. Alt's work was supported by NSF Grant EAR-080900.

References

Abbate, E., Bortolotti, V., Principi, G., 1980. Apennine ophiolites: a peculiar oceanic crust. Ofioliti, Special Issue on Tethyan Ophiolites 1, 59–96.

Abbate, E., Bortolotti, V., Passerini, P., Principi, G., Treves, B., 1994. Oceanisation processes and sedimentary evolution of the northern Apennine ophiolite suite: a discussion. Memorie della Societa Geologica Italiana 48.

Agrinier, P., Cannat, M., 1997. Oxygen-isotope constraints on serpentinization processes in ultramafic rocks from the mid-Atlantic ridge (23°N). Proceeding of the Ocean Drilling Program, Scientific Results 153, 381–388.

Agrinier, P., Cornen, G., Beslier, M.O., 1996. Mineralogical and oxygen isotopic features of serpentinites recovered from the ocean/continent transition in the Iberia Abyssal Plain. Proceeding of the Ocean Drilling Program, Scientific Results 149, 541–552.

Allen, D.E., Seyfried, J.W.E., 2003. Compositional controls on vent fluids from ultramafic-hosted hydrothermal systems at mid-ocean ridges: an experimental study at 400 °C, 500 bars. Geochimica et Cosmochimica Acta 67 (8), 1531–1542.

Allen, D.E., Seyfried, J.W.E., 2004. Serpentinization and heat generation: constraints from Lost City and Rainbow hydrothermal systems. Geochimica et Cosmochimica Acta 68 (6), 1347–1354.

Alperin, M.J., Hoehler, T.M., 2009. Anaerobic methane oxidation by archaea/sulfate-reducing bacteria aggregates: 2. Isotopic constraints. American Journal of Science 309 (10), 958–984.

Alt, J.C., Shanks, W.C.I., 1998. Sulfur in serpentinized oceanic peridotites: serpentinization processes and microbial sulfate reduction. Journal of Geophysical Research 103, 9917–9929.

Alt, J.C., Shanks, W.C.I., 2003. Serpentinization of abyssal peridotites from the MARK area, Mid-Atlantic Ridge: sulfur geochemistry and reaction modeling. Geochimica et Cosmochimica Acta 67, 641–653.

Alt, J.C., Teagle, D.A.H., 1999. The uptake of carbon during alteration of ocean crust. Geochimica et Cosmochimica Acta 63 (10), 1527–1535.

Alt, J.C., Shanks, W.C., Bach, W., Paulick, H., Garrido, C.J., Beaudoin, G., 2007. Hydrothermal alteration and microbial sulfate reduction in peridotite and gabbro exposed by detachment faulting at the Mid-Atlantic Ridge, 15° 20′ N (ODP Leg 209): a sulfur and oxygen isotope study. Geochemistry, Geophysics, Geosystems 8 (8).

Andreani, M., Mevel, C., Boullier, A.M., Escartin, J., 2007. Dynamic control on serpentine crystallization in veins: constraints on hydration processes in oceanic peridotites. Geochemistry, Geophysics, Geosystems 8.

Andreani, M., Luquot, L., Gouze, P., Godard, M., Hoisé, E., Gibert, B., 2008. Experimental study of carbon sequestration reactions controlled by the percolation of CO_2-rich brine through peridotites. Environmental Science & Technology 43, 1226–1231.

Bach, W., Garrido, C.J., Paulick, H., Harvey, J., Rosner, M., 2004. Seawater–peridotite interactions: first insights form ODP Leg 209, MAR 15°N. Geochemistry, Geophysics, Geosystems 5 (9), 22.

Bach, W., Rosner, M., Jöns, N., Rausch, S., Robinson, L.F., Paulick, H., Erzinger, J., 2011. Carbonate veins trace seawater circulation during exhumation and uplift of mantle rock: Results from ODP Leg 209. Earth and Planetary Science Letters 311, 242–252.

Barbieri, M., Masi, U., Tolomeo, L., 1979. Stable isotope evidence for a marine origin of ophicalcite from the north-central Apennines (Italy). Marine Geology 30, 193–204.

Barrett, T.J., Friedrichsen, H., 1989. Stable isotopic composition of atypical ophiolites from East Liguria, Italy. Chemical Geology 80, 71–84.

Bauer, J.E., 2002. Carbon isotopic composition of DOM. In: Hansell, D.A., Carlson, C.A. (Eds.), Biogeochemistry of Marine Dissolved Organic Matter. Academic Press, pp. 405–455.

Beard, J.S., Hopkinson, L., 2000. A fossil, serpentinization-related hydrothermal vent, Ocean Drilling Program Leg 173, Site 1068 (Iberia Abyssal Plain): some aspects of mineral and fluid chemistry. Journal of Geophysical Research 105, 16527–16539.

Berndt, M.E., Allen, D.E., Seyfried, J., W.E., 1996. Reduction of CO_2 during serpentinization of olivine at 300 °C and 500 bar. Geology 24, 351–354.

Bideau, D., Hebert, R., Hekinian, R., Cannat, M., 1991. Metamorphism of deep-seated rocks from the Garrett ultrafast transform (east pacific rise near 13°25′). Journal of Geophysical Research 96 (B6), 10079–10099.

Borthwick, J., Harmon, R.S., 1982. A note regarding CIF_3 as an alternative to BrF5 for oxygen isotope analysis. Geochimica et Cosmochimica Acta 46 (9), 1665–1668.

Boschi, C., Dini, A., Früh-Green, G.L., Kelley, D.S., 2008. Isotopic and element exchange during serpentinization and metasomatism at the Atlantis Massif (MAR 30°N): insights from B and Sr isotope data. Geochimica et Cosmochimica Acta 72 (7), 1801–1823.

Brazelton, W.J., Schrenk, M.O., Kelley, D.S., Baross, J.A., 2006. Methane- and sulfur-metabolizing microbial communities dominate the Lost City hydrothermal field ecosystem. Applied and Environmental Microbiology 72 (9), 6257–6270.

Brazelton, W.J., Sogin, M.L., Baross, J.A., 2010. Multiple scales of diversification within natural populations of archaea in hydrothermal chimney biofilms. Environmental Microbiology Reports 2 (2), 236–242.

Brazelton, W.J., Mehta, M.P., Kelley, D.S., Baross, J.A., 2011. Physiological differentiation within a single-species biofilm fueled by serpentinization. mBio 2 (4).

Cannat, M., Bideau, D., Bougault, H., 1992. Serpentinized peridotites and gabbros in the Mid-Atlantic Ridge axial valley at 15°37′N and 16°52′N. Earth and Planetary Science Letters 109 (1–2), 87–106.

Cannat, M., Fontaine, F., Escartin, J., 2010. Serpentinization and associated hydrogen and methane fluxes at slow spreading ridges. In: Rona, P.A., Devey, C.W., Dyment, J., Murton, B.J. (Eds.), Diversity of Hydrothermal Systems on Slow Spreading Ocean Ridges. Geophysical Monograph. American Geophysical Union, Washington.

Carbotte, S., Scheirer, D.S., 2004. Variability of ocean crustal structure created along the global mid-ocean ridge. In: Davis, E.E., Elderfield, H. (Eds.), Hydrogeology of the Oceanic Lithosphere. Cambridge University Press.

Charlou, J.L., Fouquet, Y., Bougault, H., Donval, J.P., Etoubleau, J., Jean-Baptiste, P., Dapoigny, A., Appriou, P., Rona, P.A., 1998. Intense CH_4 plumes generated by serpentinization of ultramafic rocks at the intersection of the 15°20′N fracture zone and the Mid-Atlantic Ridge. Geochimica et Cosmochimica Acta 62 (13), 2323–2333.

Charlou, J.L., Donval, J.P., Fouquet, Y., Jean-Baptiste, P., Holm, N., 2002. Geochemistry of high H_2 and CH_4 vent fluids issuing from ultramafic rocks at the Rainbow hydrothermal field (36°14′N, MAR). Chemical Geology 191, 345–359.

Cipolli, F., Gambardella, B., Marini, L., Ottonello, G., Zuccolini, M.V., 2004. Geochemistry of high-pH waters from serpentinites of the Gruppo di Voltri (Genova, Italy) and reaction path modeling of CO_2 sequestration in serpentinite aquifers. Applied Geochemistry 19, 787–802.

Clayton, R.N., Mayeda, T.K., 1963. The use of bromine pentafluoride in the extraction of oxygen from oxides and silicates for isotopic analysis. Geochimica et Cosmochimica Acta 27, 43–52.

Coplen, T.B., Kendall, C., Hopple, J., 1983. Comparison of stable isotope reference samples. Nature 302 (5905), 236–238.

Cortesogno, L., 1981. Carta geologica delle ofioliti del Bracco tra Lèvanto e Velva. S.E.L.C.A., Firenze.

Cortesogno, L., Galbiati, B., Principi, G., 1980. Le brecce serpentinitiche giurassiche della Liguria orientale. Symposium "On tectonic inclusions and associated rocks in serpentinites", Geneva, Switzerland. Archives des Sciences Geneva 33, 185–200.

Cortesogno, L., Galbiati, B., Principi, G., 1987. Note alla "Carta geologica delle ofioliti del Bracco" e ricostruzione della paleogeografia Giurassico-Cretacica. Ofioliti 12, 261–342.

de Wit, M.J., Hart, R.A., Hart, R.J., 1987. The Jamestown Ophiolite Complex, Barberton mountain belt: a section through 3.5 Ga oceanic crust. Journal of African Earth Sciences 6 (5), 681–730.

Delacour, A., Früh-Green, G.L., Bernasconi, S.M., Schaeffer, P., Kelley, D.S., 2008. Carbon geochemistry of serpentinites in the Lost City Hydrothermal System (30°N, MAR). Geochimica et Cosmochimica Acta 72, 3681–3702.

Desmurs, L., Manatschal, G., Bernoulli, D., 2001. The Steinmann trinity revisited: exhumation and magmatism along an ocean–continent transition: the Platta nappe, eastern Switzerland. In: Wilson, R.C.L., Whitmarsh, R.B., Taylor, B.E., Froitzheim, N. (Eds.), Non-Volcanic Rifting of Continental Margins: A Comparison of Evidence from Land and Sea. Geological Society, London, pp. 235–266.

Dick, H.J.B., Tivey, M.A., Tucholke, B.E., 2008. Plutonic foundation of a slow-spreading ridge segment: oceanic core complex at Kane Megamullion, 23°30′ N, 45°20′ W. Geochemistry, Geophysics, Geosystems 9.

Douville, E., Charlou, J.L., Oelkers, E.H., Bienvenu, P., Jove Colon, C.F., Donval, J.P., Fouquet, Y., Prieur, D., Appriou, P., 2002. The Rainbow vent fluids (36° 14′N, MAR): the influence of ultramafic rocks and phase separation on trace metal content in Mid-Atlantic Ridge hydrothermal fluids. Chemical Geology 184, 37–48.

Druffel, E.R.M., Williams, P.M., Bauer, J.E., Ertel, J.R., 1992. Cycling of dissolved and particulate organic matter in the open ocean. Journal of Geophysical Research 97, 15639–15659.

Elsgaard, L., Isaksen, M.F., Jorgensen, B.B., Alayse, A.M., Jannasch, H.W., 1994. Microbial sulfate reduction in deep-sea sediments at the Guaymas Basin hydrothermal vent area — influence of temperature and substrates. Geochimica et Cosmochimica Acta 58 (16), 3335–3343.

Falkowski, P., Scholes, R.J., Boyle, E., Canadell, J., Canfield, D., Elser, J., Gruber, N., Hibbard, K., Högberg, P., Linder, S., Mackenzie, F.T., Moore III, B., Pedersen, T., Rosenthal, Y., Seitzinger, S., Smetacek, V., Steffen, W., 2000. The global carbon cycle: a test of our knowledge of earth as a system. Science 290 (5490), 291–296.

Fouquet, Y., Charlou, J.L., Ondréas, H., Radford-Knöery, J., Donval, J.P., Douville, E., Appriou, R., Cambon, P., Pellé, H., Landuré, J.Y., NOrmand, A., Ponsevera, E., German, C.R., Parson, L., Barriga, F., Costa, I.M.A., Relvas, J., Ribeiro, A., 1997. Discovery and first submersible investigations on the Rainbow hydrothermal field on the MAR (36°14′N). Eos, Transactions of the American Geophysical Union 78 (F832).

Friedman, I., O'Neil, J.R., 1977. Compilation of stable isotope fractionation factors of geochemical interest. Data of Geochemistry. U.S. Geological Survey 440-KK.

Früh-Green, G.L., Weissert, H., Bernoulli, D., 1990. A multiple fluid history recorded in Alpine ophiolites. Journal of the Geological Society of London 147, 959–970.

Früh-Green, G.L., Plas, A., Lécuyer, C., 1996. Petrologic and stable isotope constraints on hydrothermal alteration and serpentinization of the EPR shallow mantle at Hess Deep (Site 895). Proceeding of the Ocean Drilling Program, Scientific Results 147, 255–291.

Früh-Green, G.L., Kelley, D.S., Bernasconi, S.M., Karson, J.A., Ludwig, K.A., Butterfield, D.A., Boschi, C., Proskurowski, G., 2003. 30,000 years of hydrothermal activity at the Lost City vent field. Science 301, 495–498.

Früh-Green, G.L., Connelly, J.A., Plas, A., Kelley, D.S., Grobéty, B., 2004. Serpentinization of oceanic peridotites: implications for geochemical cycles and biological activity. The Subseafloor Biosphere at Mid-Ocean Ridges, 144. American Geophysical Union, Washington D.C.

Gerlach, T.M., 1989. Degassing of carbon dioxide from basaltic magma at spreading centers: II. Mid-oceanic ridge basalts. Journal of Volcanology and Geothermal Research 39 (2–3), 221–232.

Gibson, I.L., Milliken, K.L., Morgan, J.K., 1996. Serpentinite-breccia landslide deposits generated during crustal extension at the Iberian margin. In: Whitmarsh, R.B., Sawyer, D.S., Klaus, A., Masson, D.G. (Eds.), Proceeding of the Ocean Drilling Program, Scientific Results, pp. 571–575.

Hopkinson, L., Beard, J.S., Boulter, C.A., 2004. The hydrothermal plumbing of a serpentinite-hosted detachment: evidence from the West Iberia non-volcanic rifted continental margin. Marine Geology 204, 301–315.

Ito, E., Clayton, R.N., 1983. Submarine metamorphism of gabbros from the Mid-Cayman rise: an oxygen isotopic study. Geochimica et Cosmochimica Acta 47 (3), 535–546.

Jamtveit, B., Putnis, C., Malthe-Sorenssen, A., 2009. Reaction induced fracturing during replacement processes. Contributions to Mineralogy and Petrology 157 (1), 127–133.

Jamtveit, B., Kobchenko, M., Austrheim, H., Malthe-Sorenssen, A., Royne, A., Svensen, H., 2011. Porosity evolution and crystallization-driven fragmentation during weathering of andesite. Journal of Geophysical Research 116, B12204.

Kampschulte, A., Strauss, H., 2004. The sulfur isotopic evolution of Phanerozoic seawater based on the analysis of structurally substituted sulfate in carbonates. Chemical Geology 204, 255–286.

Karson, J.A., Lawrence, R.M., 1997. Tectonic setting of serpentinite exposures on the western median valley wall of the MARK area in the vicinity of site 920. Proceeding of the Ocean Drilling Program, Scientific Results 153, 5–22.

Kelemen, P.B., Matter, J., 2008. In situ carbonation of peridotite for CO_2 storage. Proceedings of the National Academy of Sciences of the United States of America 105 (45), 17295–17300.

Kelley, S.D., Karson, J.A., Blackman, D.K., Früh-Green, G.L., Butterfield, D.A., Lilley, D.M., Olson, E.J., Schrenk, M.O., Roell, K.K., Lebon, G.T., Rivizzigno, P., the AT3-60 Shipboard Party, 2001. An off-axis hydrothermal vent field near the Mid-Atlantic Ridge at 30°N. Nature 412, 145–149.

Kelley, D.S., Karson, J.A., Früh-Green, G.L., Yoerger, D.R., Shank, T.M., Butterfield, D.A., Hayes, J.M., Schrenk, M.O., Olson, E.J., Proskurowski, G., Jakuba, M., Bradley, A., Larson, B., Ludwig, K.A., Glickson, D., Buckman, K., Bradley, A.S., Brazelton, W.J., Roe, K., Elend, M.J., Delacour, A., Bernasconi, S.M., Lilley, D.M., Baross, J.A., Summons, R.E., Sylva, S.P., 2005. A serpentinite-hosted ecosystem: the lost city hydrothermal field. Science 307, 1428–1434.

Klein, F., Garrido, C.J., 2011. Thermodynamic constraints on mineral carbonation of serpentinized peridotite. Lithos 126, 147–160.

Konn, C., Charlou, J.L., Donval, J.P., Holm, N.G., Dehairs, F., Bouillon, S., 2009. Hydrocarbons and oxidized organic compounds in hydrothermal fluids from Rainbow and Lost City ultramafic-hosted vents. Chemical Geology 258, 299–314.
Kyser, T.K., 1986. Stable isotope variations in the mantle. In: Valley, J.W., Taylor, H.P., O'Neil, J.R. (Eds.), Stable Isotopes in High Temperature Geological Processes. Reviews in Mineralogy. Mineralogical Society of America, pp. 141–164.
Lackschewitz, K.S., Armini, M., Augustin, N., Dubilier, N., Edge, D., Engemann, G.M.F., Felden, J., Franke, P., Gärtner, A., Garbe-Schönberg, D., Gennerich, H.-H., Hüttig, D., Marbler, H., Meyerdierks, A., Pape, T., Perner, M., Reuter, M., Ruhland, G., Schmidt, K., Schott, T., Schroeder, M., Schroll, G., Seiter, C., Stecher, J., Strauss, H., Viehweger, M., Weber, S., Wenzhöfer, F., Zielinski, F., 2005. Longterm study of hydrothermalism and biology at the Logatchev field, Mid-Atlantic Ridge at 14°45′ N (revisit 2005; HYDROMAR II). Cruise Report.
Lagabrielle, Y., Cannat, M., 1990. Alpine Jurassic ophiolites resemble the modern central Atlantic basement. Geology 18 (4), 319–322.
Lavoie, D., Cousineau, P.A., 1995. Ordovician ophicalcites of southern Quebec Appalachians — a proposed early sea-floor tectonosedimentary and hydrothermal origin. Journal of Sedimentary Research 65, 337–347.
Lemoine, M., 1980. Serpentinites, gabbros and ophicalcites in the Piemont–Ligurian domain of the western Alps — possible indicators of oceanic fracture-zones and of associated serpentinite protrusions in the Jurassic–Cretaceous Tethys. Archives des Sciences 33 (2–3), 103–115.
Lemoine, M., Tricart, P., Boillot, G., 1987. Ultramafic and gabbroic ocean floor of the Ligurian Tethys (Alps, Corsica, Apennines): in search of a genetic model. Geology 15, 622–625.
Lever, M.A., Rouxel, O., Alt, J.C., Shimizu, N., Ono, S., Coggon, R.M., Shanks III, W.C., Lapham, L., Elvert, M., Prieto-Mollar, X., Hinrichs, K., Inagaki, F., Teske, A., 2013. Evidence for microbial carbon and sulfur cycling in deeply buried ridge flank basalt. Science 339, 1305–1308.
Londry, K.L., Des Marais, D.J., 2003. Stable carbon isotope fractionation by sulfate-reducing bacteria. Applied and Environmental Microbiology 69 (5), 2942–2949.
Ludwig, K.A., Kelley, D.S., Butterfield, D.A., Nelson, B.K., Früh-Green, G.L., 2006. Formation and evolution of carbonate chimneys at the Lost City Hydrothermal Field. Geochimica et Cosmochimica Acta 70, 3625–3645.
Macdonald, A.H., Fyfe, W.S., 1985. Rate of serpentinization in seafloor environments. Tectonophysics 116 (1–2), 123–135.
Marroni, M., Pandolfi, L., 2007. The architecture of an incipient oceanic basin: a tentative reconstruction of the Jurassic Liguria-Piemonte basin along the Northern Apennines–Alpine Corsica transect. International Journal of Earth Sciences 96, 1059–1078.
Martin, B., Fyfe, W.S., 1970. Some experimental and theoretical observations on the kinetics of hydration reactions with particular reference to serpentinization. Chemical Geology 6, 185–202.
Martin, W., Russell, M.J., 2007. On the origin of biochemistry at an alkaline hydrothermal vent. Philosophical Transactions of the Royal Society of London. Series B, Biological Sciences 362 (1486), 1887–1925.
Matter, J.M., Kelemen, P.B., 2009. Permanent storage of carbon dioxide in geological reservoirs by mineral carbonation. Nature Geoscience 2 (12), 837–841.
Mattey, D., Lowry, D., Macpherson, C., 1994. Oxygen isotope composition of mantle peridotite. Earth and Planetary Science Letters 128 (3–4), 231–241.
McCollom, T.M., 1999. Methanogenesis as a potential source of chemical energy for primary biomass production by autotrophic organisms in hydrothermal systems on Europa. Journal of Geophysical Research 104 (E12), 30729–30742.
McCollom, T.M., 2007. Geochemical constraints on sources of metabolic energy for chemolithoautotrophy in ultramafic-hosted deep-sea hydrothermal systems. Astrobiology 7 (6), 933–950.
Mével, C., 2003. Serpentinization of abyssal peridotites at mid-ocean ridges. Comptes Rendus Geosciences 335 (10–11), 825–852.
Molli, G., 1995. Pre-orogenic high temperature shear zones in an ophiolite complex (Bracco massif, Northern Apennines, Italy). In: Vissers, R.L.M., Nicolas, A. (Eds.), Mantle and Lower Crust Exposed in Oceanic Ridges and in Ophiolites. Kluwer Academic Publishers, Dordrecht, Netherlands, pp. 147–161.
Muehlenbachs, K., Clayton, R.N., 1976. Oxygen isotope composition of oceanic-crust and its bearing on seawater. Journal of Geophysical Research 81 (23), 4365–4369.
O'Hanley, D.S., 1996. Serpentinites: Records of Tectonic and Petrological History. Oxford Monographs on Geology and Geophysics. Oxford University Press, New York, Oxford 34.
Palandri, J.L., Reed, M.H., 2004. Geochemical models of metasomatism in ultramafic systems: serpentinization, rodingitization, and sea floor carbonate chimney precipitation. Geochimica et Cosmochimica Acta 68 (5), 1115–1133.
Plas, A., 1997. Petrologic and Stable Isotope Constraints on Fluid–Rock Interaction, Serpentinization and Alteration of Oceanic Ultramafic Rocks. ETH Zurich, Zurich.
Proskurowski, G., Lilley, M.D., Kelley, D.S., Olson, E.J., 2006. Low temperature volatile production at the Lost City hydrothermal field, evidence from a hydrogen stable isotope geothermometer. Chemical Geology 229, 331–343.
Proskurowski, G., Lilley, M., Seewald, J., Früh-Green, G.L., Olson, E.J., Lupton, J.E., Sylva, S.P., Kelley, D.S., 2008. Abiogenic hydrocarbon production at Lost City hydrothermal field. Science 319, 604–607.
Rampone, E., Piccardo, G.B., 2000. The ophiolite-oceanic lithosphere analogue: new insights from the Northern Apennines (Italy). Ophiolite and Oceanic Crust: New Insights from Field Studies and Ocean Drilling Program, 349: Geol. Soc. Am. Spec. Pap (21-34 pp.).
Sakai, R., Kusakabe, M., Noto, M., Ishii, T., 1990. Origin of waters responsible for serpentinization of the Izu-Ogasawara-Mariana forearc seamounts in view of hydrogen and oxygen isotope ratios. Earth and Planetary Science Letters 100 (1–3), 291–303.
Savin, S.M., Lee, M.C., 1988. Isotopic studies of phyllosilicates. In: Bailey, S.W. (Ed.), Hydrous Phyllosilicates. Reviews in Mineralogy. Mineralogical Society of America, pp. 189–223.
Sawyer, D.S., Whitmarsh, R.B., Klaus, A., et al., 1994. Iberia Abyssal Plain Sites 897–901, 149. Proceedings of the Ocean Drilling Program, Initial Reports. Ocean Drilling Program, College Station, TX.
Schrenk, M.O., Kelley, D.S., Bolton, S.A., Barossa, J.A., 2004. Low archaeal diversity linked to subseafloor geochemical processes at the Lost City hydrothermal field, Mid-Atlantic Ridge. Environmental Microbiology 6 (10), 1086–1095.
Schroeder, T., John, B., Frost, B.R., 2002. Geologic implications of seawater circulation through peridotite exposed at slow-spreading mid-ocean ridges. Geology 30 (4), 367–370.
Schroeder, T., Cheadle, M.J., Dick, H.J.B., Faul, U., Casey, J.F., Kelemen, P.B., 2007. Nonvolcanic seafloor spreading and corner-flow rotation accommodated by extensional faulting at 15 degrees N on the Mid-Atlantic Ridge: A structural synthesis of ODP Leg 209. Geochemistry, Geophysics, Geosystems 8.
Schulte, M., Blake, D., Hoehler, T., McCollom, T., 2006. Serpentinization and its implications for life on the early Earth and Mars. Astrobiology 6 (2), 364–376.
Schwarzenbach, E.M., 2011. Serpentinization, fluids and life: comparing carbon and sulfur cycles in modern and ancient environments. ETH Zurich, Thesis No. 19588, Zurich. (240 pp.).
Schwarzenbach, E.M., Früh-Green, G.L., Bernasconi, S.M., Alt, J.C., Shanks III, W.C., Gaggero, L., Crispini, L., 2012. Sulfur geochemistry of peridotite-hosted hydrothermal systems: comparing the Ligurian ophiolites with oceanic serpentinites. Geochimica et Cosmochimica Acta 91, 283–305.
Shilobreeva, S., Martinez, I., Busigny, V., Agrinier, P., Laverne, C., 2011. Insights into C and H storage in the altered oceanic crust: results from ODP/IODP Hole 1256D. Geochimica et Cosmochimica Acta 75 (9), 2237–2255.
Siegenthaler, U., Sarmiento, J.L., 1993. Atmospheric carbon dioxide and the ocean. Nature 365, 119–125.
Smith, D.K., Escartin, J., Schouten, H., Cann, J.R., 2008. Fault rotation and core complex formation: Significant processes in seafloor formation at slow-spreading mid-ocean ridges (Mid-Atlantic Ridge, 13°–15°N). Geochemistry, Geophysics, Geosystems 9.
Stetter, K.O., 1996. Hyperthermophilic prokaryotes. FEMS Microbiology Reviews 18, 149–158.
Strating, H., 1991. The evolution of the Piemonte-Ligurian ocean: a structural study of ophiolite complexes in Liguria (NW Italy). Geologica Ultraiectina, 74. Instituut voor Aardwetenschappen der Rijksuniversiteit Utrecht, Utrecht.
Surour, A.A., Arafa, E.H., 1997. Ophicarbonates: calcified serpentinites from Gebel Mohagara, Wadi Ghadir area, Eastern Desert, Egypt. Journal of African Earth Sciences 24 (3), 315–324.
Takai, K., Nakamura, K., Toki, T., Tsunogai, U., Miyazaki, M., Miyazaki, J., Hirayama, H., Nakagawa, S., Nunoura, T., Horikoshi, K., 2008. Cell proliferation at 122 °C and isotopically heavy CH_4 production by a hyperthermophilic methanogen under high-pressure cultivation. Proceedings of the National Academy of Sciences of the United States of America 105 (31), 10949–10954.
Taylor, H.P., 1968. The oxygen isotope geochemistry of igneous rocks. Contributions to Mineralogy and Petrology 19, 1–71.
Taylor, H.P., 1984. Oxygen and hydrogen isotope studies of hydrothermal interactions at submarine subaerial spreading centers. In: Rona, P.A., Boström, K., Laubier, L., Smith, K.L. (Eds.), Hydrothermal Processes at Seafloor Spreading Centers. Plenum Press, New York, pp. 83–139.
Treves, B.E., Harper, G.D., 1994. Exposure of serpentinites on the ocean floor: sequence of faulting and hydrofracturing in the northern Apennine Ophicalcite. Ofioliti 19b (435-466).
Treves, B., Kickmott, D., Vaggelli, G., 1995. Texture and microchemical data of oceanic hydrothermal calcite veins, northern Apennine ophicalcite. Ofioliti 20 (2), 111–122.
Trudinger, P.A., Chambers, L.A., Smith, J.W., 1985. Low-temperature sulfate reduction — biological versus abiological. Canadian Journal of Earth Sciences 22 (12), 1910–1918.
Weissert, H.J., Bernoulli, D., 1985. A transform margin in the Mesozoic Tethys: evidence from the Swiss Alps. Geologische Rundschau 74 (3), 665–679.
Wenner, D.B., Taylor, H.P., 1971. Temperatures of serpentinization of ultramafic rocks based on $^{18}O/^{16}O$ fractionation between coexisting serpentine and magnetite. Contributions to Mineralogy and Petrology 32, 165–185.
Wenner, D.B., Taylor, H.P., 1973. Oxygen and hydrogen isotope studies of serpentinization of ultramafic rocks in oceanic environments and continental ophiolite complexes. American Journal of Science 273, 207–239.
Whitmarsh, R.B., Sawyer, D.S., 1996. The ocean/continent transition beneath the Iberia Abyssal Plain and continental-rifting to seafloor-spreading processes. Proceeding of the Ocean Drilling Program, Scientific Results 149, 713–733.
Whitmarsh, R.B., Wallace, P.J., 2001. The rift-to-drift development of the West Iberia nonvolcanic continental margin: a summary and review of the contribution of ocean drilling program Leg 173. Proceeding of the Ocean Drilling Program, Scientific Results 173, 1–36.
Whitmarsh, R.B., Beslier, M.-O., Wallace, P.J., et al., 1998. Return to Iberia Sites 1065–1070, 173. Proceedings of the Ocean Drilling Program, Initial Reports. Ocean Drilling Program, College Station, TX.
Whitmarsh, R.B., Manatschal, G., Minshull, T.A., 2001. Evolution of magma-poor continental margins from rifting to seafloor spreading. Nature 413 (6852), 105–154.
Wilson, R.C.L., 2001. Non-Volcanic Rifting of Continental Margins: A Comparison of Evidence from Land and Sea. Geological Society Special Publication, London 187.